Title

Management of Hsp90-Dependent Protein Folding by Small Molecules Targeting the Aha1 Co-Chaperone

Journal

Cell Chemical Biology, 27(3)

ISSN

2451-9456

Authors

Singh, Jay K
Hutt, Darren M
Tait, Bradley
et al.

Publication Date

2020-03-01

DOI

10.1016/j.chembiol.2020.01.008

Peer reviewed

HHS Public Access

Author manuscript

Cell Chem Biol. Author manuscript; available in PMC 2021 March 19.

Published in final edited form as:

Cell Chem Biol. 2020 March 19; 27(3): 292–305.e6. doi:10.1016/j.chembiol.2020.01.008.

Management of Hsp90-Dependent Protein Folding by Small Molecules Targeting the Aha1 Co-Chaperone

Jay K. Singh[1], **Darren M. Hutt**[1], **Bradley Tait**[2], **Naihsuan C. Guy**[3], **Jeffrey C. Sivils**[3], **Nina R. Ortiz**[3], **Ashley N Payan**[3], **Shravan Kumar Komaragiri**[4], **Jazzmin Jovonna Owens**[4], **David Culbertson**[5], **Laura J. Blair**[6], **Chad Dickey**[6,#], **Szu Yu Kuo**[7], **Dan Finley**[8], **H. Jane Dyson**[5], **Marc B. Cox**[3], **Jaideep Chaudhary**[4], **Jason E. Gestwicki**[7], **William E. Balch**[1,9,*]

[1]Department of Molecular Medicine, Skaggs Institute of Chemical Biology, The Scripps Research Institute La Jolla, CA, USA 92037

[2]Brad Tait Enterprise LLC, 80 Christian Way North Andover, MA, USA 01845

[3]Department of Biological Sciences and Border Biomedical Research Center, University of Texas at El Paso, El Paso, TX, USA 79902

[4]School of Arts and Sciences, Clark Atlanta University, Atlanta, GA, USA 30314

[5]Department of Integrative Structural and Computational Biology, The Scripps Research Institute, La Jolla, CA, USA 92037

[6]Department of Molecular Medicine and Byrd Alzheimer's Research Institute, University of South Florida, Tampa, FL, USA, USA 33613

[7]Department of Pharmaceutical Chemistry, University of California San Francisco, San Francisco, CA, USA 94158

[8]Department of Cell Biology, Harvard Medical School, Boston, MA, USA 02115

[9]Lead Contact

Summary

[*]Correspondence: webalch@scripps.edu.

[#]Deceased

Author Contributions

JKS performed the ASH high throughput screen and validation, the *in vitro* characterization of SEW84. BT designed all SEW84 derivatives for SAR studies. DMH and WEB wrote the manuscript and interpreted the data. NCG, NRO, ANP and JCS performed the glucocorticoid and androgen receptor assays in the laboratory of MCB. SKK and JJO performed the cell proliferation studies of prostate cancer cell lines in the laboratory of JC. CD provided all data pertaining to the clearance of phosphorylated tau. DC performed all the NMR in the laboratory of HJD. SYK performed the tau high content imaging and mRNA analysis in the laboratory of JEG. DF provided the data for the combined action of SEW84 with IU47 on tau clearance.

Declaration of Interests

A provisional patent (Docket # 1361.254PRV) on SEW84 and its derivatives has been filed by Scripps Research on behalf of JKS, BT & WEB. Patents 8933087 and 9201073 are held on IU1, IU1-47 for USP14 inhibition, filed by Harvard University on behalf of DF and others. IU1 and IU1-47 patents have been licensed to Proteostasis Therapeutics.

Hsp90 plays an important role in health and is a therapeutic target for managing misfolding disease. Compounds that disrupt co-chaperone delivery of clients to Hsp90 target a subset of Hsp90 activities, thereby minimizing the toxicity of pan-Hsp90 inhibitors. Herein, we have identified SEW04784 as a first-in-class inhibitor of the Aha1-stimulated Hsp90 ATPase activity without inhibiting basal Hsp90 ATPase. Nuclear magnetic resonance analysis reveals that SEW84 binds to the C-terminal domain of Aha1 to weaken its asymmetric binding to Hsp90. Consistent with this observation, SEW84 blocks Aha1-dependent Hsp90 chaperoning activities including the *in vitro* and *in vivo* refolding of Firefly Luciferase, the transcriptional activity of the androgen receptor in cell-based models of prostate cancer and promotes the clearance of phosphorylated tau in cellular and tissue models of neurodegenerative tauopathy. We propose that SEW84 provides a novel lead scaffold for developing therapeutic approaches to treat proteostatic disease.

In Brief

Singh *et al* identified SEW84 as an inhibitor of the stimulated Hsp90 activity. SEW84 is able to reduce the expression and activity of androgen receptor variants associated with prostate cancer. SEW84 preferentially clears phosphorylated, aggregation prone Tau, found in a number of neurodegenerative diseases such as Alzheimer's disease.

Graphical Abstract

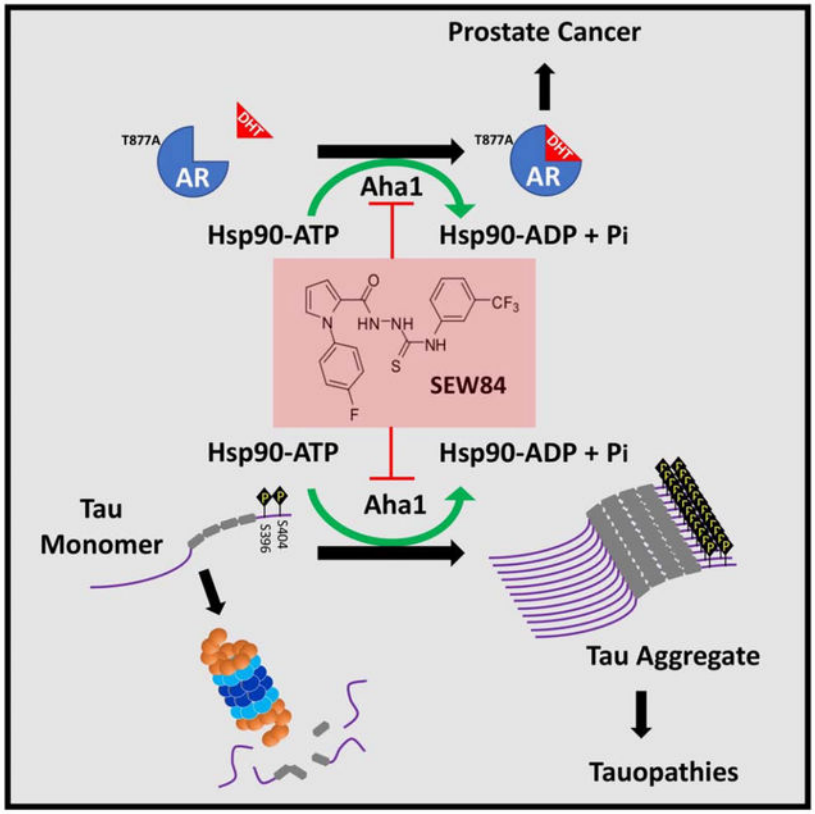

Keywords

Heat shock protein 90 (Hsp90); Aha1; tau; Alzheimer's Disease; androgen receptor (AR); Prostate Cancer

Introduction

Variant protein structures are managed by proteostasis components (Balch et al., 2008, Balchin et al., 2016, Sala et al., 2017), which include heat shock protein (Hsp) 90, which reach an expression level of 2–5% of total protein (Coppinger et al., 2012). Hsp90 is an essential (Geller et al., 2018, Karras et al., 2017, Queitsch et al., 2002, Sahasrabudhe et al., 2017, Schopf et al., 2017) ATP-dependent molecular chaperone which, together with its regulatory co-chaperones and the Hsp70 complex, form the cellular machinery regulating protein folding and function (Geller et al., 2018, Schopf et al., 2017). Given the ubiquitous role of Hsp90 in folding, we must learn how to manage disease-associated roles of Hsp90 while sparing the normal function.

Hsp90 exists as a homodimer, with each protomer composed of 4 domains: an N-terminal ATP binding domain (NTD), the middle domain (MD), which is involved in client and co-chaperone binding and ATP hydrolysis, a linker which connects the NTD and MD and a C-terminal domain (CTD) involved in dimerization and recruitment of tetracopeptide repeat (TPR) containing co-chaperones (Schopf et al., 2017, Verba and Agard, 2017). The Hsp90 dimer undergoes a series of structural rearrangements during its ATPase cycle. In the nucleotide-free (apo) form, the C-terminally dimerized Hsp90 adopts an open conformation, which closes upon ATP hydrolysis, a process that promotes protein folding. The entire Hsp90 folding cycle is assisted by the action of multiple co-chaperones (Geller et al., 2018, Schopf et al., 2017, Verba and Agard, 2017), including the accelerator of Hsp90 ATPase (Aha1) (Horvat et al., 2014, Koulov et al., 2010, Lepvrier et al., 2015, Rehn and Buchner, 2015, Shelton et al., 2017, Synoradzki and Bieganowski, 2015, Tripathi et al., 2014, Wolmarans et al., 2016).

Aha1 is a two domain protein conserved from yeast to man (Rehn and Buchner, 2015, Wolmarans et al., 2016, Wortmann et al., 2017). It contributes to the activation of specific client proteins, including kinases, steroid hormone receptors and transcription factors (Li et al., 2012, Sahasrabudhe et al., 2017, Schopf et al., 2017, Taipale et al., 2010), by stimulating the ATPase activity of Hsp90 (Koulov et al., 2010, Li et al., 2013a, Retzlaff et al., 2010). The binding of Aha1 to Hsp90 is asymmetric (Koulov et al., 2010), bridging the MD of one protomer with the NTD of the other to promote NTD dimerization and ATPase stimulation (Koulov et al., 2010, Li et al., 2013a, Retzlaff et al., 2010). The silencing of Aha1 decreases client protein activation and increases cellular sensitivity to Hsp90 inhibitors (Hsp90i) (Koulov et al., 2010). In cystic fibrosis (CF), a reduction of Aha1 expression corrects the trafficking defect associated with the deletion of Phe508 (F508del) variant of the CF transmembrane conductance regulator (CFTR) (Wang et al., 2006). These data suggest an important role for a reduced ATPase activity in the stabilization of Hsp90-dependent client proteins involved in oncological and neurodegenerative diseases.

Numerous Hsp90is have been developed, including geldanamycin (GA) and radicicol, which compete with ATP for the binding at the NTD of Hsp90 thereby blocking its ATPase activity (Roe et al., 1999, Schulte et al., 1998). While they have been the subject of many clinical trials, none have had success due to toxicity associated with globally inhibiting Hsp90 (Glaze et al., 2005, Wang et al., 2016). To circumvent this issue, inhibitors that disrupt co-chaperone binding have been developed including novobiocin (Cohen et al., 2012, Hall et al., 2016, Kusuma et al., 2012, Samadi et al., 2011, Zhang et al., 2012, Zhang et al., 2018, Zhao and Blagg, 2013), which are expected to only disrupt a subset of Hsp90 activities. Recently, compounds have been identified that disrupt Aha1 stimulated Hsp90 ATPase activity (Ihrig and Obermann, 2017, Stiegler et al., 2017), although their ability to directly interact with Aha1 remains to be determined.

We have identified a novel Aha1 binding Hsp90 inhibitor SEW04784 (SEW84) that alter the Aha1-stimulated Hsp90 (ASH) ATPase activity without inhibiting the basal ATPase of Hsp90. We show that SEW84 exhibits therapeutic potential by blocking the transcriptional activity of prostate cancer (PCa) associated androgen receptor (AR) variants and exhibits the ability to preferentially clear toxic, phosphorylated tau species associated with tauopathies, such as Alzheimer's disease (AD).

Results

Identifying inhibitors of ASH activity

To identify molecules that inhibit ASH activity, we adapted an assay based on the ability of colored products to quench the inherent fluorescence of white microtiter plates (Zuck et al., 2005). In brief, P_i, originating from the Hsp90-mediated ATP hydrolysis, is complexed with molybdate ($(NH_4)_6Mo_7O_{24}$) to form phosphomolybdate ($(NH_4)_3PMo_{12}O_{40}$) (Figure 1A), which then binds quinaldine red (QR) to form a colored product that quenches the fluorescence of white microtiter plates (Figure 1A). Here, compounds that inhibit the ATPase activity of Hsp90 will produce less P_i and exhibit less quenching (Figure 1B).

Our assay yielded a Z' factor of 0.7, indicating suitability for high throughput screening (Zhang et al., 1999). Screening of the 16,000 compound Maybridge library yielded 131 compounds that inhibited ASH activity with ≥ 3 SD of the DMSO control (Figure 1B). GA failed to completely inhibit the ASH activity in our screen (Figure 1B) due to pre-binding of Hsp90 to Aha1 permitting an initial round of ATP hydrolysis before compounds can prevent further ATPase activity. A secondary screen resulted in 35 confirmed compounds. A potent inhibitor of the ASH activity without inhibiting basal Hsp90 ATPase in the absence of Aha1 was identified as SEW84. A structurally similar compound, SEW04777 (SEW77), had undetectable activity in the ASH assay, and will serve as a negative control (Figure 1D).

SEW84 specifically inhibits Aha1-stimulated activity

A titration of SEW84 revealed complete inhibition of ASH activity at 5 μM (Figure 2A) and an IC_{50} of 0.3 μM (Figure 2B), similar to that seen with GA (Figure 2B). Importantly, SEW84 did not affect the basal ATPase of Hsp90 (Figure 2A, C).

We also monitored the impact of SEW84 on the binding of Hsp90 to Aha1. To monitor this protein-protein interaction (PPI), we labeled Aha1 with acrylodan, a cysteine-labeling dye whose fluorescence is sensitive to the local environment. The fluorescence of acrylodan-labeled full length Aha1 (ac-Aha1) increases with increasing concentration of Hsp90 (Figure 2D), yielding a dissociation constant (K_d) of 1.1 ± 0.1 μM. The addition of SEW84 reduces the ac-Aha1 fluorescence, resulting in a 50% increase in the K_d value (1.7 ± 0.2 μM) (Figure 2D), suggesting that SEW84 weakens the Hsp90-Aha1 interaction. We only observe a partial reduction in the binding affinity of Hsp90 for Aha1 (Figure 2D), which is due to Aha1 needing to bind to both the MD and NTD of Hsp90 to stimulate Hsp90 ATPase activity (Koulov et al., 2010, Retzlaff et al., 2009). Since our in vitro binding assay will not distinguish between Aha1 bound to a single or both binding sites, the binding data reflects the ability of these two proteins to interact at one of the sites even if binding at the other site is disrupted. SEW84 did not affect the ATPase activity of the Hsp70 chaperone complex (Figure 2E), suggesting that SEW84 is not a general ATPase inhibitor.

SEW84 binds to the CTD of Aha1

All known Hsp90i, including radicicol and GA as well as the recently discovered ASH inhibitor, HAM1, have been reported to induce significant structural changes in Hsp90 (Stiegler et al., 2017). Therefore we assessed if SEW84 bound directly to Hsp90 by monitoring its tryptophan (Trp) fluorescence. We observed a linear increase in fluorescence with increasing concentration of Hsp90 in the presence of either DMSO and 25 μM SEW84 (Figure 2F) indicating that SEW84 does not bind to Hsp90, a conclusion consistent with the observation that SEW84 does not inhibit the basal ATPase activity of Hsp90.

To address if SEW84 binds to Aha1, we acquired transverse relaxation optimized spectroscopy (TROSY) ^{1}H-^{15}N HSQC NMR spectra of ^{15}N-labeled Aha1. The addition of SEW84 to full-length Aha1 caused many cross peak shifts in the spectrum, indicating that the compound binds to Aha1 in a localized area (Figure 3A and Figure S1A). Given that Aha1 is a 2-domain protein (Koulov et al., 2010, Meyer et al., 2004), the location of residues affected by SEW84 was further assessed by examining the TROSY-HSQC spectra of the isolated NTD (1–163) and CTD (164–338) of Aha1 in the presence and absence of SEW84. SEW84 did not cause any changes in the spectrum of the isolated NTD (Figure 3B and Figure S1B), but significant chemical shifts were observed in the CTD of Aha1 (Figure 3C and Figure S1C). Our analysis revealed that there are 24 amino acids that exhibit spectral shifts in response to SEW84 (Figure S1D). These include 5 residues (K277, S278, W279, H283 and F284) that map to the Aha1 region previously shown to interact with Hsp90 (^{276}FKSWPEGHFATITL^{289}) (Koulov et al., 2010) (Figure S1E).

To confirm that SEW84 binds to the CTD of Aha1, we monitored its impact on the fluorescence of acrylodan-labeled Aha1. We observed a dose-dependent fluorescence quenching of the acrylodan-labeled full length Aha1 in the presence of SEW84 (Figure 3D) with a Kd of 1.74 μM. While SEW84 had no impact on Ac-NTD-Aha1, we did observed a dose-dependent quenching of Ac-CTD-Aha1 in the presence of SEW84 (Figure 3E) which exhibited a Kd of 0.4 μM. SEW84 also disrupts the binding of the isolated CTD of Aha1 to Hsp90, resulting in an increase in the Kd for this PPI (Figure 3F). These data indicate that

the NTD of Aha1 will bind to the MD of Hsp90 independent of the presence of SEW84 and the reduced Kd reflects the loss of binding between the CTD-Aha1 with the NTD-Hsp90 thereby reducing the overall strength of the Aha1-Hsp90 binding and completely inhibiting the ASH activity (Koulov et al., 2010, Retzlaff et al., 2010). These data agree with the mechanistic action of Celastrol, which inhibits Hsp90 by binding to and disrupting the structure of cdc37 and p23, thereby interfering with their ability to regulate Hsp90 (Chadli et al., 2010, Sreeramulu et al., 2009).

SEW84 impedes the re-folding of firefly luciferase (FLuc)

To address whether the ability of SEW84 to inhibit the ASH activity affects Hsp90 client proteins, we monitored its effect on the refolding of denatured firefly luciferase (FLuc) *in vitro*. Thermal denaturation of FLuc reduces its luminescence, an effect that can be reversed by the addition of the 6P chaperone complex (Figure 4A). The refolding of FLuc is dependent on the presence of the Hsp70 chaperone, as evidenced by the ability of the Hsp70-inhibitor, JG98 (Li et al., 2013b), to completely block the refolding of FLuc. The refolding potential of the 6P chaperone machinery is also dependent on Hsp90 as evidence by the impact of geldanamycin (GA), which reduces FLuc folding by 25% (Figure 4A). Bacterial and mammalian Hsp90 and Hsp70 chaperones are capable of refolding FLuc alone (Moran Luengo et al., 2018) and that the ATP-dependent step occurs early in refolding, predicting that GA and SEW84 would not impact FLuc refolding. The data also showed a 4-fold higher demand for Hsp90 relative to HtpG to achieve maximal FLuc activity (Moran Luengo et al., 2018), suggesting that differences in the basal ATPase activity of these chaperones (Graf et al., 2009, McLaughlin et al., 2004) might be responsible and that ATPase stimulating co-chaperones might contribute to the folding of FLuc. In agreement with this hypothesis, we observed that SEW84 causes a 25% reduction in FLuc refolding (Figure 4A), suggesting that the Hsp90-sensitive refolding of Fluc is dependent on Aha1.

We also assessed the impact of SEW84 on the folding of FLuc variants *in vivo*. We studied WT and the L5 (R188Q) and L33 (R188Q/R261Q) FLuc variants, whose mutations disrupt polar contacts in the protein, thereby affecting their stability (Gupta et al., 2011). SEW84 caused a dose-dependent decrease in active WT-FLuc above 5 μM (Figure 4B). This effect was more pronounced on the L5 and L33 variants, where we observed a dose-dependent loss of activity at 0.5 μM, with L5 retaining significantly more activity than L33 at increasing doses (Figure 4B). We did not observe any SEW84-associated toxicity (Figure 4C) suggesting that the loss of FLuc activity was not due to cytotoxic effects. Therefore, SEW84 is capable of inhibiting ASH activity in the complex environment of the cell.

SEW84 inhibits the activity of steroid hormone receptors

Aha1-Hsp90 plays important roles in folding and function of steroid hormone receptors (SHR) (Harst et al., 2005), which are linked to numerous diseases. Thus, we monitored the ability of SEW84 to modulate the activity of the glucocorticoid receptor (GR) (Figure S2) and AR (Figure 5A) in MDA-kb2 cells stably expressing the appropriate SHR responsive FLuc reporters. We observed that SEW84 inhibited the GR- and AR-dependent luciferase expression with IC_{50} values of 1.3 μM (Figure S2) and 0.7 μM (Figure 5A), respectively, values similar to that seen for the FKBP52-specific AR inhibitor MJC13(De Leon et al.,

2011) (Figure 5A), and better than that of the Hsp90i 17-AAG (Figure 5A). Importantly, the non-functional SEW84 analog, SEW77, did not impact the AR-dependent expression of FLuc (Figure 5A). These *in vivo* IC_{50} values are in line with the *in vitro* IC_{50} (0.3 μM) (Figure 2B) and K_d (1.7 μM) (Figure 4A) values for the respective SEW84-mediated inhibition of Hsp90 ATPase and binding to Aha1.

Mutations in the AR are associated with PCa (Baker et al., 2018). The T877A mutation results in an AR that can be activated by non-cognate steroids, allowing prostate cells to continue to grow in the face of androgen deprivation therapy (ADT) and chemical castration (Elo et al., 1995, Grigoryev et al., 2000, Miyamoto et al., 1998, Tan et al., 1997). We therefore monitored the impact of SEW84 on LNCaP cells, a prostate cancer cell line homozygous for the T877A-AR variant. We observed a dose-dependent inhibition of the expression and secretion of the prostate specific antigen (PSA) (Figure 5B), an AR-responsive gene used as a biomarker for the onset and progression of PCa. While we did not see a difference in the ability of SEW84 and SEW77 to inhibit the proliferation of LNCaP cells in the presence of the synthetic androgen, R1881 (Figure 5C), we did observe a synergistic decrease in LNCaP cell proliferation when we combined 1 μM GA with 10 μM SEW84 (Figure 5D). This effect was not observed when combining the low dose of GA with SEW77 (Figure 5D).

In addition to missense mutations, deletion of the ligand binding domain (ΔLBD) of the AR leads to constitutively active variants responsible for aggressive forms of PCa. These mutations are insensitive to ADT and are currently without treatment. To address if SEW84-mediated inhibition of Hsp90 would have any impact on ΔLBD variants, we monitored its impact on 22Rv1 cells that express both a dihydrotestosterone (DHT) responsive variant and ΔLBD-AR variant. SEW84 inhibited both the constitutive and DHT-responsive secretion of PSA (Figure 5E). We observed that SEW84 induced a dose dependent decrease in the expression of both full length (FL) and ΔLBD-AR in the presence of R1881, whereas SEW77 only exhibited statistically significant effects on FL and ΔLBD-AR at the non-therapeutic dose of 100 μM (Figure 5F). We observed a similar result in the absence of R1881 (data not shown). We also observed that in the absence of R1881, SEW84 is able to inhibit the proliferation of 22Rv1 cells at 10 and 100 μM, whereas SEW77 only exhibited a statistically significant impact on the proliferation of these cells at 100 μM (Figure 5G), consistent with their respective effects on the expression of FL- and ΔLBD-AR. Conversely, SEW84 did not affect the proliferation of 22Rv1 cells in the presence of R1881 (Figure 5H), despite a clear effect on the expression of AR protein (Figure 5F). The residual expression of FL-AR in these cells is likely sufficient to sustain an R1881-mediated proliferation of these cells. Our data highlights the benefit of SEW84 in the treatment of PCa associated with constitutively active, truncated AR variants or for patients having undergone ADT, however a more long term analysis would be required to assess its impact on patients which have not undergone ADT.

Analysis of the Structure Activity Relationship (SAR) of SEW84

We performed an SAR analysis to assess the structural components of SEW84 that contribute to its ASH inhibitory activity (Figure S3 **& Suppl Analytical Report of A90 SAR compounds**).

We observed that removing the meta trifluoromethyl on phenyl ring 2 caused a significant reduction in ASH activity (compare SEW84 vs A90–2 and −3 vs −4) (Figure 6, S3 & S4) while removing the fluorine group in the first phenyl ring (A90–3) had no impact (Figure 6, S3 & S4). Replacing the hydrazinecarbanothioamide (C=S) with a hydrazinecarbanocarbonyl group (C=O) caused a significant reduction in activity (compare SEW84 to A90–10) (Figure 6, S3 & S4), an effect that is consistent with the inactive analogue, SEW77 (Figure 1D). Secondly. converting the hydrazinecarbothioamide linker to triazole (A90–11) reduced the activity of SEW84 (Figure 6, S3 & S4), suggesting that the flexibility of the linker is required for proper engagement of Aha1, which may not be permitted with the more rigid triazole structure.

By fixing the para-fluorophenyl in ring 1, we were able to show a trend for smaller groups on ring 2 to be less potent inhibitors of ASH activity (OMe > CF_3 ~ CH_3, > CN, > F > H) with no trend for electron donating groups (EDG) vs electron withdrawing groups (EWG). Additionally, moving the trifluoromethyl from meta to ortho (A90–5) decreased the potency of the molecule (Figure 6, S3 & S4) while moving it to the para position (A90–6) caused a slight increase in ASH inhibitory activity (Figure 6, S3 & S4). The para trifluoromethyl substitution was further evaluated with EWG, EDG, and varying sizes as was carried out for the meta position. Changing it to fluorine (A90–13), methoxy (A90–14) or nitrile (A90–15) groups yield slightly more active molecules (Figure 6, S3 & S4), however, changing it to a methyl (A90–12) reduced its potency to that of A90–2 (Figure 6, S3 & S4). As in the meta position there was no trend for EDG vs EWG substitutions.

Combining the more functional groups at the para and meta positions on the second phenyl ring had varying effects. While the addition of a methyl group (A90–17) to the meta position of A90–6 completely inhibited the activity of the molecule (Figure 6, S3 & S4), the addition of another trifluoromethyl (A90–18) or methoxy (A90–19) increased the activity of the parent molecule by 50% (Figure 6, S3 & S4). Moving the para fluorine group in ring one to the meta position (A90–20) significantly reduced activity (Figure 6, S3 & S4) while moving it to the ortho position had no effect (A90–21) (Figure 6, S3 & S4). Replacing the fluorine group with methyl (A90–22, A90–23, A90–24) resulted in molecules with similar activity to SEW84 (Figure 6, S3 & S4).

Taken as a whole, the SAR data highlight the importance of the thiocarbonyl for the ability of SEW84 to function as an inhibitor of ASH. Additionally, we observed that substituents on the phenyl rings, particularly in the para and meta positions, can be used to modulate the potency of SEW84, however we observed no consistent trend for the ability of EDG or EWG to impact the potency of SEW84.

SEW84 can reduce the expression of phospho-tau

Tau (*MAPT*) is a microtubule associated protein (MAP) that promotes and stabilizes the formation of axonal microtubules (Drubin and Kirschner, 1986). Mutations or hyperphosphorylation of tau (p-tau) leads to altered microtubule binding culminating in the loss of axonal transport (Hong et al., 1998) and tau aggregation (von Bergen et al., 2000). This latter effect is a hallmark of a series of neurodegenerative diseases termed tauopathies, the most prominent of which is Alzheimer's disease (AD), where p-tau aggregates can be found in neurofibrillary tangles, senile plaques and cellular processes (Hong et al., 1998). p-Tau aggregates have been shown to be sensitive to the protective action of heat shock proteins (Luo et al., 2007), where Hsp70i and Hsp90i or modulating the expression of regulatory co-chaperones can mediate the clearance of p-tau in cells (Dickey et al., 2006, Dickey et al., 2007, Jinwal et al., 2009, Luo et al., 2007, Pratt et al., 2015, Young et al., 2018).

We used HEK293 cells transfected with a doxycycline (Dox) inducible GFP-tagged 0N4R-tau to monitor the impact of SEW84 on tau aggregation using high content imaging, where a reduction in GFP would indicate a reduction in cellular tau. SEW84 and its active analogs reduced cellular tau levels (Figure 7A & S5), whereas inactive SEW84 analogs (SEW77, A90–2, −5, −16 and −20) had a reduced ability to clear tau (Figure 7A, & S5). Thus, the *in vitro* and *in vivo* SAR data are consistent. None of the SEW84 analogues reduced the mRNA levels of GFP-tau, suggesting that the reduced Tau levels occur post-translationally (Figure 7B).

We observed that SEW84, but not SEW77, preferentially reduced WT-0N4R p-tau (Figure 7C) as early as 1 h post treatment (Figure S6A), a result consistent with previous observations showing that Hsp90is can selectively clear p-tau species (Dickey et al., 2007, Dickey et al., 2006). We confirmed that SEW84 preferentially targets p-tau using a Phos-tag PAGE, which allows for the separation of phosphorylated subpopulations of a protein of interest by supplementing the phosphate binding, 1,3-bis[bis(pyridin-2-ylmethyl)amino]propan-2-olato dimanganese(II) complex (Mn^{2+}-Phos-Tag) into the separation gel of an SDS-PAGE (Kinoshita et al., 2014, Kinoshita et al., 2009). The reversible binding of the phosphate groups of a protein with the Mn^{2+}-Phos-Tag additive leads to altered migration of phosphoproteins on an SDS-PAGE, with more highly phosphorylated proteins exhibiting slower migration than lesser and unphosphorylated proteins (Kinoshita et al., 2009, Kinoshita et al., 2014) (Figure S6B). We observe that SEW84 preferentially clears p-tau species (black arrows) over non-phosphorylated species (grey arrows) in a dose-dependent manner. We also observed that SEW84, but not SEW77, reduced Aha1 binding to tau (Figure 7D) without reducing Hsp90 binding. While we did observe a slight increase in Hsp90 expression levels (Figure 7D), reminiscent of a mild heat shock response, we did not observe cytotoxicity at doses that promote the clearance of p-tau.

We used HEK293 cells expressing RFP-tagged 0N4R-tau treated with proteosomal inhibitors, which leads to the formation of RFP-positive perinuclear aggregates (Figure 7E, **white arrows**) (Guthrie and Kraemer, 2011). SEW84 is able to completely abrogate the aggregation of tau (Figure 7E).

To translate these observations to a more physiologically relevant model, we assessed the impact of SEW84 on p-tau in primary rat cortical neurons expressing endogenous WT-tau. The treatment of rat cortical neurons with SEW84, but not SEW77, resulted in an ~50% reduction in p-tau (pS396/S404) levels but only a 30% reduction in total tau (Figure S6C–E). The effect of SEW84 was equipotent to IU1–47, an inhibitor of the deubiquitinating enzyme, USP14, which has been shown to clear tau (Figure S6C–E) (Boselli et al., 2017). Combining these 2 treatments yielded a synergistic effect on the clearance of p-tau (Figure S6C–D). We also observed a dose-dependent reduction in the levels of p-tau (pS396/S404) in cultured brain slices from 4-month-old transgenic mouse (rTg4510), expressing tau-P301L, a variant shown to disrupt microtubule binding (Hasegawa et al., 1998) and increase aggregation(Figure 7F).

Discussion

Herein, we describe the discovery and characterization of a novel inhibitor of the ASH ATPase activity, SEW84. The chaperoning activity of Hsp90 was first established using SHRs (Pratt and Dittmar, 1998) such as the AR, which is involved in the pathology of PCa. The standard of care for this disease includes ADT to remove the source of androgens and abrogate the growth of prostatic tissue. ADT eventually fails resulting in CRPC due to AR overexpression, mutations conferring ADT resistance, enhanced co-regulator expression or activity and intratumoral production of androgen. While the treatment with abiraterone, a CYP17A1 inhibitor, to block the intratumoral synthesis of androgen (Attard et al., 2008), and enzalutamide, an AR-LBD antagonist (Tran et al., 2009), are designed to slow the growth of CRPC, many patients are refractory to these treatments or quickly develop resistance (Antonarakis et al., 2014). Therefore, the development of therapeutic options which can inhibit androgen responsive AR variants as well as AR variants associated with CRPC are critical for extending the lifespan of affected individuals. A further level of complication arises from the observations that in many cases of CRPC with AR truncation variants, there is a concomitant increased expression of the GR which has the capacity to modulate the expression of many AR responsive genes in prostate cells (Arora et al., 2013, Sahu et al., 2013), thus providing a way for these transformed cells to escape growth arrests mediated by ADT. Herein, we showed that SEW84 inhibits the *in vivo* transcriptional activity of WT- GR as well as WT and PCa-associated AR variants, including a ΔLBD-AR variant which has been shown to be refractory to classical Hsp90is (Gillis et al., 2013, Shafi et al., 2013). These results support the interpretation that the therapeutic activity of SEW84 is directly related to its targeting of the ASH activity, which is critical for priming AR function.

Hsp90 is critical for the biogenesis and functional cycling of numerous clients proteins (https://www.picard.ch/Hsp90Int/index.php) (Echeverria et al., 2011), with the microtubule associated protein, tau, being one of the best characterized (Dickey et al., 2007, Karagoz et al., 2014), with Hsp90is emerging as therapeutic options for the treatment of tauopathies (Mok et al., 2018, Pratt et al., 2015, Young et al., 2018). While these compounds eliminate toxic p-tau aggregates, clinical translation of these results has not been observed, largely due to cytotoxicity of pan-Hsp90is (Glaze et al., 2005, Iyer et al., 2012). To circumvent this toxic effects, recent efforts have turned to targeting the Hsp90 co-chaperones. The silencing of

most co-chaperones impedes the ability of Hsp90is to clear p-tau species (Dickey et al., 2007), suggesting that it is the Hsp90 complex which needs to be targeted rather than individual Hsp90 molecules, a hypothesis supported by the observation that PU-H71, a Hsp90i, targets the hyperconnected chaperome (Joshi et al., 2018, Kishinevsky et al., 2018, Rodina et al., 2016). Indeed, Aha1 is critical for the Hsp90-mediated aggregation of p-tau species and inhibiting its Hsp90 binding prevents the formation of *de novo* aggregates and promotes the clearance of p-tau (Shelton et al., 2017). Consistent with these observations, SEW84 promotes the clearance and aggregation of toxic p-tau species. Taken together, these data suggest that the normal ASH activity protects p-tau, leading to its aggregation. Alterations in the ability of Hsp90 to bind ATP, as seen with Hsp90is, to adopt a stabilized ATP-bound state, as seen with p23 silencing (Dickey et al., 2007), or to hydrolyze ATP, as seen with small molecules that target Aha1 association with Hsp90 (Stiegler et al., 2017) and shown herein, lead to the clearance of p-tau. We posit that inhibiting Aha1 directly has the benefit of not altering the basal chaperoning function of Hsp90, thereby mitigating the cytotoxic issues seen with other Hsp90is (Glaze et al., 2005, Wang et al., 2016). This hypothesis is consistent with our observation that the silencing of Aha1 corrects the trafficking of the cystic fibrosis (CF) associated variant of the CF transmembrane conductance regulator (CFTR) protein, F508del(Wang et al., 2006), while the treatment of these same cells with GA, leads to rapid cell death. Thus, an Aha1 specific inhibitor presents a therapeutic opportunity for treating neurodegenerative diseases.

While Aha1 is often considered only as a co-chaperone activator of Hsp90 ATPase, the majority of Aha1 exists in an Hsp90-free state in human cells even though it is found at concentration of $1/1000^{th}$ that of Hsp90 (Tripathi et al., 2014). This may be explained by its catalytic co-chaperone activity, which would be expected to shift the binding equilibrium of the Hsp90/Aha1 interaction to the non-bound state. On the other hand, Aha1 has been shown to possess chaperoning activity by preventing the aggregation of both FLuc and Rhodanese *in vitro* and *in vivo* in the absence of Hsp90. While the ability of Aha1 to bind to its clients has been shown to require the first 22 amino acids located at the NTD of Aha1 (Li et al., 2013a), which is unaffected by SEW84, the ATPase stimulating activity *in vitro* required the full-length protein. These data suggest that while SEW84 is unlikely to disrupt the ability of Aha1 to bind to its client proteins, its binding to the CTD of Aha1 could impact its chaperoning activity, thereby promoting the clearance of bound clients, such as p-tau and the AR, through ubiquitination, as shown for tau in response to co-incubation with IU1–47 (Boselli et al., 2017) or for Aha1-bound, heat denatured FLuc in the absence of chaperone-mediated refolding (Tripathi et al., 2014). Therefore, the ability of SEW84 to mediate a reduction in tau aggregation and block the activity of AR variants could be the concerted action of inhibiting both the ASH and chaperone activities of Aha1. Its impact on truncated AR variants may be explained by its latter function when AR is lacking the Hsp90 interaction site. While our data shows that SEW84 binds to the CTD of Aha1 weakening Hsp90-Aha1 binding and thereby inhibiting ASH activity, we cannot rule out possible effects on other Hsp90 co-chaperones that might have complementary binding motifs to that of Aha1. This possible dependence of SEW84 on targeting a particular Hsp90 containing chaperome could explain the ability of A90–10 and A90–17 to reduce GFP-tau expression *in vivo*, while exhibiting no inhibitory properties in our *in vitro* ASH assay.

Our results highlight the potential benefits of Aha1-targeted co-chaperone inhibitors in managing human misfolding disease. Such compounds allow the cell to maintain the basal activity of Hsp90, potentially mitigating the cytotoxic effects reported with the use of Hsp90is (Glaze et al., 2005, Iyer et al., 2012). We have previously suggested that the proteostasis environment is critical in establishing set-points to manage protein folding states in response to variation in the human population (Wang and Balch, 2018). Our results herein suggest that Aha1 is a regulator of these set-points in health, aging, and disease.

STAR Methods

LEAD CONTACT AND MATERIALS AVAILABILITY

Further information and requests for resources should be directed to and will be fulfilled by the Lead Contact, William E. Balch (webalch@scripps.edu). All unique/stable reagents generated in this study are available from the Lead Contact with a completed Materials Transfer Agreement. Some of the reagents may be limited due to our need to maintain an adequate supply.

EXPERIMENTAL MODEL AND SUBJECT DETAILS

Cell Models—MDA-kb2 cells were derived from the breast cancer cell line, MDA-MB-453 by stable transfection with a mouse mammary tumor virus (MMTV) luciferase-neo reporter gene construct for gluococorticoid receptor and androgen receptor detection. The cell line originated from a 48 year old Caucasian female adult. LNCaP cells are a prostate cancer cell line derived from left supraclavicular lymph node metastatic site in a 50 year old Caucasian male adult. 22Rv1 cells are a human (male) prostate carcinoma epithelial cell line derived from a xenograft that was serially propagated in mice after castration-induced regression and relapse of the parental, androgen-dependent CWR22 xenograft. HeLa cells are an adenocarcinoma cell line derived from a 31 year old black female adult and HEK 293 cells are derived from human (female) embryonic kidney cells. HeLa cells and HEK293 cells are stably to express 0N4R-tau. Primary cortical neurons were prepared from whole cerebral cortices of day 18 Sprague-Dawley rat embryos. The maintenance details for each cell line are listed in the Method Details below.

Mouse Models—The brain slices in this study originated from 4-month-old transgenic rTg4510 mice (female) which express human 0N4R-P301L tau linked with familial frontotemporal dementia (FTD).

METHOD DETAILS

Expression and purification of human Hsp90β—An overnight culture of BL-21 (DE3) *E.* coli carrying the pET14b plasmid containing the human Hsp90β (pET-90β) cDNA was diluted into 2 liter of Luria Broth (LB) medium containing carbenicillin (100 g/ml) and grown at 37°C to an optical density (OD) of 0.8 (~5 h). The *E. coli* cells harboring pET-90β plasmid were induced by 1 mM isopropyl β-D-thiogalactoside (IPTG) at 20°C for 16 h. Pellete d cells were resuspended in 40 ml of immobilized metal affinity chromatography (IMAC) buffer A (20 mM NaH2PO4 pH 8, 500 mM NaCl, 1 mM MgOAc, and 5 mM β-mercaptoethanol (β-ME)) supplemented with a EDTA-free protease inhibitor tablet (Roche

Diagnostics). The cells were then lysed on ice by sonication at 40% power for 3x for 20 s with a 30s recovery between each sonication burst. The lysate was centrifuged at 25 000xg for 50 min in a type 70 Ti rotor (Beckman Coulter), and the supernatant was fractionated over a 5 ml Ni^{2+}-charged HiTrap Chelating HP column (GE Healthcare) using an AKTA FPLC with Frac-950 fraction collector (GE Healthcare). Gradient fractionation was carried out with IMAC buffer B (IMAC A with 1 M imidazole). Hsp90β containing fractions were pooled, concentrated using an Amicon Ultra-15 Centrifugal Filter Unit with Ultracel-50 membrane, MWCO: 50,000 (Millipore), and further gradient fractionated on an 8-ml Mono-Q HR 10/10 column, (GE Healthcare) using Mono-Q buffer A (20 mM Tris, pH 7.5, and 1 mM DTT), and Mono Q buffer B (20 mM Tris, pH 7.5, 1 M NaCl, and 1 mM DTT). Hsp90β containing fractions were collected and concentrated to a minimal volume (0.5 ml) using an Amicon Ultra-15. The concentrated sample was passed through gel filtration chromatography (GFC) using Hi-load™ 16/60 Superdex 200 prep grade (GE Healthcare) in 40 mM HEPES/KOH, pH 7.5, 300 mM KCl, 1 mM EDTA, and 1 mM DTT. Final purity was ≥98% based on SDS-PAGE.

Expression and purification of human Aha1—An overnight culture of BL-21 (DE3) *E.* coli carrying the pET14b plasmid containing the human Aha1 (pET-Aha1) cDNA was diluted into 2 liter LB medium containing carbenicillin (100 μg/ml) and grown at 37°C to an OD of 0.8 (~5h). The cells were induced by 0.5 mM IPTG at 30°C for 5 h. After induction, the cells were pelleted and stored at −80°C. Pelleted cells were resuspende d in 40 ml of immobilized metal affinity chromatography (IMAC) buffer A (50 mM Tris-HCl pH 8, 500 mM KCl, and 5 mM β-ME) supplemented with a protease inhibitor tablet. Cell lysis and HiTrap Chelating HP column and Mono-Q column purification were performed as described above. Aha1 containing fractions were pooled, concentrated, and further fractionated by high performance gel filtration chromatography using a Superdex™ 75 HR 10/30 (Amersham Biosciences) in 40 mM HEPES, pH 7.5, 50 mM KCl, 2 mM $MgCl_2$ and 1 mM DTT. Final purity was ≥98% based on SDS-PAGE. Purified Hsp90β and Aha1 were aliquoted and snap-frozen in liquid Nitrogen prior to storage at −80°C.

Expression and purification of human Hsp70—Recombinant Hsp70 was expressed in BL21(DE3) and harvested by lysis in buffer A (20 mM Hepes, pH 7, 1 mM EDTA, 1 mM DTT, 0.5 mM PMSF) supplemented with 25 mM KCl. Hsp70 was purified by sequential chromatography first on Q-Sepharose (Amersham Pharmacia Biotech) and then on ATP agarose (SigmaAldrich). The resulting protein was precipitated with 75% (NH4)2SO4 in the presence of 10 mM EDTA to promote the dissociation of ATP. Hsp70 was further purified by size exclusion chromatography on Superose S-300 (Amersham Pharmacia Biotech) in buffer A containing 100 mM KCl, followed by chromatography on Q-Sepharose. Hsp70 was eluted with a 25–250-mM KCl linear gradient in buffer A (200 ml, 1 ml/min). The molar extinction coefficient, ε1% = 6.2, was used to quantify Hsp70 (Chang et al., 2002).

Expression and purification of human Hsp40—An overnight culture of BL-21 (DE3) *E.* coli carrying the pET14b plasmid containing the human Hsp40 (pET-Hsp40) cDNA was diluted into 2 liter LB medium containing carbenicillin (100 μg/ml) and grown at 37°C to an OD of 0.8 (~5h). The cells were induced by 0.5 mM IPTG at 30°C for 5 h. After

induction, the cells were pelleted and stored at −80°C. Pelleted cells were resuspende d in 40 ml of immobilized metal affinity chromatography (IMAC) buffer A (50 mM Tris-HCl pH 8, 500 mM KCl, and 5 mM β-ME) supplemented with a protease inhibitor tablet. Cell lysis and HiTrap Chelating HP column and Mono-Q column purification were performed as described above. Hsp40 containing fractions were pooled, concentrated, and further fractionated by high performance gel filtration chromatography using a Superdex™ 75 HR 10/30 (Amersham Biosciences) in 40 mM HEPES, pH 7.5, 50 mM KCl, 2 mM $MgCl_2$ and 1 mM DTT. Final purity was ≥98% based on SDS-PAGE. Purified Hsp40 was aliquoted and snap-frozen in liquid Nitrogen prior to storage at −80°C.

Expression and purification of Bag1—Recombinant Bag1 was expressed by BL21(DE3) cells. Cultures were grown at 37 °C for 5 h, cooled to 20 °C, and induced overnight with 200 μM isopropyl 1-thio-β-D-galactopyranoside. Bag1-expressing cells were pelleted, resuspended in His binding buffer (50 mM Tris, 300 mM NaCl, and 10 mM imidazole (pH 8.0)) and protease inhibitor tablets (Roche), and then sonicated. Supernatants were incubated with Ni-NTA resin for 2 h at 4 °C, washed with binding buffer, His wa shing buffer (50 mM Tris, 300 mM NaCl, and 30 mM imidazole (pH 8.0)), and finally eluted with His elution buffer (50 mM Tris, 300 mM NaCl, and 300 mM imidazole (pH 8.0)). After Ni-NTA columns, sample was subjected to tobacco etch virus (TEV) protease cleavage overnight and dialyzed into MonoQ buffer A (20 mM HEPES, 10 mM NaCl, and 15 mM β-ME (pH 7.6)). Protein sample was applied to a MonoQ column (GE Healthcare) and eluted by a linear gradient of MonoQ buffer B (buffer A + 1 M NaCl). Fractions were concentrated and applied to a Superdex S200 (GE Healthcare) size exclusion column in Bag-1 buffer (25 mM HEPES, 5 mM MgCl2, and 150 mM KCl (pH 7.5)) (Rauch and Gestwicki, 2014).

Expression and purification of HOP—Hop were subcloned into pET28a for expression of untagged proteins in BL21(DE3) cells. BL21(DE3) cells lysates were then purified by three-step chromatography (AKTA FPLC, Amersham Biosciences). Briefly, BL21(DE3) cells lysates were fractionated by HiPrep 16/10 Heparin-Sepharose chromatography followed by Resource Q-FPLC and 16/60 Superdex 200 FPLC. Final peak fractions for Hop were pooled and concentrated using Amicon Centricon-10 filters (Millipore) (Carrigan et al., 2006).

Expression and purification of p23—p23 is expressed by BL21(DE3) cells. After a 3-h induction with 1 mM 1-thio-β-D-galactopyranoside, the bacteria were pelleted and washed with phosphate-buffered saline, pH7.4. The pellets were resuspended in 10 mM Tris-HCl (pH 7.5), 1 mM EDTA, 10 mM monothioglycerol and were sonicated. The soluble extract was applied to a DEAD-cellulose column. A 0–0.5M KCl gradient elution resulted in the isolation of highly purified p23 (>90% pure). Fractions containing p23 were dialyzed into 10 mM Tris-HCl (pH 7.5), 50 mM KCl, 3 mM $MgCl_2$, 10 mM monothioglycerol and were concentrated to approximately 0.5 mg/ml (Weaver et al., 2000).

Quinaldine Red Assay—Based on pioneering efforts of Gestwicki (Moses et al., 2018, Chang et al., 2008), we developed a modified quinaldine red (QR) based HTS assay for screening of compounds that specifically inhibit Aha1. Quinaldine red (QR) reagent was

made by mixing 1 g ammonium molybdate, dissolved in 14 mL of 4N HCl, 43 mg QR dye dissolved in 40 mL of 1N HCl and solutions, 1.2 mL of 1% poly vinyl alcohol (PVA) and completing the volume to 100 ml with ddH_20 water. To initiate the QR assay, 2.3 μM Hsp90 and 14 μM Aha1 were added to the wells of a 384-well white microtiter plate (Greiner Bio-one) in reaction buffer (25 mM Hepes pH 7.5, 10 mM $MgCl_2$, and 1 mM DTT). The plate was subsequently centrifuged 250xg for 1 min and the proteins allowed to incubate at room temperature for 30 min. Subsequently, 50 nL of the test compounds from the Maybridge library (or DMSO vehicle) were pinned into the appropriate wells, the plate centrifuged at 250xg for 1 min and incubated at room temperature for 30 min. The reaction was initiated by adding 14 mM final concentration of ATP, the plate centrifuged at 250xg for 1 min and incubated at 37 °C for 3 h in a humidified environment. Following the 3 h reaction, plates were transferred to room temperature for 10 min and then 15 μl of QR reagent was added to each well of the plate using a Multidrop Dispenser. The ability of the QR reagent to quench the inherent fluorescence (Ex/Em 430nm/530nm) of the white microtiter plates was measured using an EnVision Multilabel Fluorescence Reader (PerkinElmer). The signal to background (S:B) ratio and Z′ factor were determined in triplicates in 384-well format. The S:B ratio was calculated using the equation: S:B = median of high control/median of low control. The low controls are those wells that have Hsp90, Aha1, ATP, and DMSO in reaction buffer, which will generate the highest amount of Pi and therefore provide the highest QR reagent-mediated quenching of fluorescence. The high controls are wells that have Aha1, ATP, and DMSO in buffer in the absence or presence of compound since they will generate the least amount of Pi and therefore provide little quenching of the fluorescence of the microtiter plates. Z' was calculated based on the equation: $Z' = 1 - 3(\sigma_H + \sigma_L)/(\mu_H - \mu_L)$, where σ and μ represent the standard error and mean for the High (H) and Low (L) controls. The percent inhibition was defined as 100 – (High Control – Test condition)/(High Control – Low Control). Inhibitors of the Aha1-stimulated Hsp90 ATPase were defined as those with percentage inhibition greater than 3 standard deviations from the low control. To validate the QR assay, we also established conditions to measure human Hsp90 ATPase activity using the Promega ADP Glo Max™ Kinase Kit according to the manufacturer's directions with identical results (data not shown).

Measurement of effect of SEW84 on the ability of Aha1 to stimulate the ATPase activity of Hsp90—Hsp90 (8 μM) was added to the wells of a 384-well plate containing reaction buffer (25 mM Hepes pH 7.5, 10 mM $MgCl_2$, and 1 mM DTT) and incubated on ice for 30 min in the absence and presence of Aha1 (16 μM). Following the incubation period, different concentrations of SEW84 (0, 0.1, 0.5, 1, and 5 μM), or its derivatives, were added to the reaction mixture and the reaction allowed to continue for an additional 30 min on ice. Subsequently, 2 mM ATP was added to the reaction mixture and the plate immediately transferred to 37 °C to initiate ATPase activity. To assess the rate of ATP hydrolysis, 7 μL aliquots were withdrawn at 0, 3, 6, 15, 30, and 60 min and transferred to the wells of a white 384 well microtiter plate containing 3 μL of EDTA (100 mM) on ice. After completion of the time course, 15 μL of the QR reagent was added to each well followed immediately by 2.5 μL of 35% sodium citrate and mixed. Kinetics of Aha1 stimulated Hsp90 ATP hydrolysis was measured using a BioTek Synergy Mx Monochromator based multi-mode plate reader.

Measurement of effect of SEW84 on the ATPase activity of Hsp70—The indicated chaperones (Hsp90 (8 μM), Hsp70 (4 μM), Hsp40 (2 μM), BAG1 (1.5 μM), HOP (0.5 μM) and Aha1 (2 μM)) were added to the wells of a 384-well plate containing reaction buffer (25 mM Hepes pH 7.5, 10 mM $MgCl_2$, and 1 mM DTT) and incubated on ice for 30 min. Following the incubation period, vehicle or 15 μM SEW84 were added to the reaction mixture and the reaction allowed to continue for an additional 30 min on ice. Subsequently, 2 mM ATP was added to the reaction mixture and the plate immediately transferred to 37 °C to initiate ATPase activity. To assess the rate of ATP hydrolysis, 7 μL aliquots were withdrawn at 0, 3, 6, 15, 30, and 60 min and transferred to the wells of a white 384 well microtiter plate containing 3 μL of EDTA (100 mM) on ice. After completion of the time course, 15 μL of the QR reagent was added to each well followed immediately by 2.5 μL of 35% sodium citrate and mixed. Kinetics of Aha1 stimulated Hsp90 ATP hydrolysis was measured using a BioTek Synergy Mx Monochromator based multi-mode plate reader.

Labeling of Aha1 with acrylodan—The cysteine residues of human Aha1 were chemically modified by a thiol reactive acrylodan (6-Acryloyl-2-Dimethylaminonaphthalene) molecular probe (Singh et al., 2007). For acrylodan labeling, Aha1 was incubated in 40 mM Hepes, pH 8.0, 50 mM KCl, 5 mM $MgCl_2$ with 5-fold molar excess of acrylodan at 4 °C for 2 0h. The reaction mixture was spun at 40000xg for 30 min at 4°C to re move any aggregate formed during reactions. The unbound acrylodan were removed by dialysis against 20 mM Hepes buffer, pH 7.5, 10 mM KCl and 1 mM DTT at 4°C for 24 h, with b uffer changes every 8 h. The concentration of Aha1 was measured at 280nm, and the concentration of Aha1-bound acrylodan (Acrylodan-Aha1) was determined by using an extinction coefficient of 20,000 $M^{-}1\ cm^{-}1$ at 392 nm. Incorporation stoichiometry was calculated by dividing acrylodan-Aha1 concentration by the Aha1 concentration. The labeling efficiency of acrylodan to Aha1 was found to be 0.8 ± 0.15.

Binding of SEW84 or Hsp90β to Aha1—Acrylodan-labeled full length or CTD-Aha1 (1 μM) was incubated with the 25 μM SEW84 in the presence or absence of different amounts of Hsp90 (0 to 10 μM) for 30 min over ice in reaction buffer (20 mM Hepes, pH 7.5, 10 $MgCl_2$, 5 mM KCl). The excitation and emission spectra were recorded at 390 nm, and 495 nm, respectively; using BioTek Synergy Mx Monochromator based multi-mode plate reader. The increased acrylodan-Aha1 signals at 495 nm upon binding to Hsp90β was used to determine the dissociation constant (Kd) of the Aha1 and Hsp90β interaction using the equation:

$$\Delta F = \Delta F_{\max} L/(K\mathrm{d} + L)$$

Where ΔF is change in the fluorescence intensity of the acrylodan-Aha1 upon binding to Hsp90β. ΔF_{max} is the maximum change in the fluorescence intensity of acrylodan-Aha1 when it is fully liganded with Hsp90β, and L is the concentration of Hsp90β. The ΔF_{max} value (50091 ± 4201) was calculated. ΔF was calculated by subtracting the fluorescence intensity of acrylodan-Aha1 in the absence of Hsp90β from the fluorescence intensity of acrylodan-Aha1 in the presence of Hsp90β (Singh et al., 2007). All the data were statistically analyzed by One-Way ANOVA and curve fitted using GraphPad software.

Tryptophan fluorescence measurements—The indicated amount of Hsp90 was mixed with DMSO (black squares) or 25 μM (black triangles) and incubated for 30 min at room temperature before collecting the tryptophan spectra (270nm/325nm) using a BioTek SynergyMx plate reader. The ΔF values were determined as described above.

NMR spectroscopy—Isotopically-labeled samples of human Aha1, Aha1(1–163) and Aha1(164–338) were prepared by expression in *E. coli* BL21 DE3 [DNAY] in M9 minimal medium containing $(^{15}NH_4)_2SO_4$ and purified according to the protocol described above. Samples were dialyzed into NMR buffer (50 mM sodium phosphate buffer pH 7.00, 150 mM NaCl, 5 mM $MgCl_2$, 2% glycerol, 2 mM DTT, 0.05% sodium azide). ^{1}H-^{15}N HSQC-TROSY spectra for full length, NTD- and CTD-Aha1 in the absence or presence of 100 μM SEW84 were acquired at 900 MHz on a Bruker Avance 900 spectrometer at 20°C.

Hsp90-Aha1 dependent refolding of FLuc—Firefly luciferase was heat denatured at 45 °C fo r 8 min in 20 mM Hepes, pH 7.6, 85 mM potassium acetate, 1 mM magnesium acetate, 1.5 mM DDT and 1 mg/ml BSA containing 10 μM human Hsp90β. The refolding of thermally inactivated luciferase was initiated by diluting it 10-fold in tubes containing an ATP regenerating system (creatine phosphokinase (3.5U/ml), phosphocreatine (10 mM) and ATP (2 mM)) and Hsp70 (4 μM), Hsp40 (2 μM), Bag1 (1.5 μM), HOP (0.5 μM), and Aha1 (2 μM), in the presence or absence of SEW84 (15 μM), GA (15 μM) or JG98 (15 μM). The reaction was carried out for 8 h at RT. Luciferase activity was measured using Promega Steady-Glo® luciferase assay system and BioTek Synergy Mx Monochromator based multi-mode plate reader. Native luciferase was set as 100% and all other values normalized to this control.

GR and AR-mediated transcription assays—MDA-kb2 cells, which stably express an androgen- and glucocorticoid-responsive firefly luciferase reporter construct, were seeded at 20,000 cells/well in 100 μl Leibovitz's L-15 medium supplemented with 10% charcoal-stripped FBS (CS-FBS) at 0% CO_2, in 96 well clear bottom plates and grown to 80% confluence. Cells were treated with 0.2 nM DHT (EC_{50} for DHT in this cell line) or 10 nM dexamethasone (DEX; EC_{50} for DEX in this cell line) and the indicated concentrations of inhibitors for 20 h. Following treatment, the cells were lysed in 100 μl of Bright-Glo Luciferase Assay System (Promega Corp., Madison, WI) and incubated at room temperature for 4 min. For luciferase activity, the light emission was measure in a luminescence plate reader (Luminoskan Ascent, Thermo Labsystems) and luminescence measurement using Bright-Glo (Promega) luciferase assay reagent according to the manufacturer's instructions.

ELISA assays for prostate specific antigen (PSA) secretion—ELISA assays to assess drug effects on PSA expression and secretion were performed in LNCaP and 22Rv1 prostate cancer cells. LNCaP cells endogenously express the AR T877A mutant (homozygous) and are sensitive to androgens. 22Rv1 cells express both full-length AR with an in-frame tandem duplication of exon 3 that encodes the second zinc finger of the AR DNA-binding domain, and a truncated AR lacking the C-terminal hormone binding domain. Thus, 22Rv1 cells are both androgen sensitive and can grow in the absence of androgens. Both LNCaP and 22Rv1 cells were maintained in MEM-EBSS (HyClone) supplemented

with 10% FBS. The Human PSA ELISA Kit (Alpha Diagnostic International, ADI) to quantify secreted PSA in the media was used. The cells were plated at a density of 2×10^5 cells per well in 12-well plates in 1 mL of respective standard growth media and incubated at 37°C with supplemental 5% CO_2. When cells were attached, they were washed three times and replaced with 1 mL of respective growth media modified by replacement of 10% FBS with 10% CS-FBS at 37°C with supplemental 5% CO_2. After 48 h, the cells were treated with DMSO + EtOH (negative control), DMSO + agonist (DHT, 50 nM for LNCaP and 1 nM for 22Rv1, positive control), or the agonist with a range of SEW84 concentrations for 24 h. For evaluating basal and hormone-induced PSA secretion in 22Rv1 cells, the aforementioned experimental conditions were used with the exception that SEW84 was tested at a single high dose (100 μM). Supernatants were collected, and the assays were performed according to manufacturer's instructions. 25 μL of standards, controls, and supernatant samples were added into appropriate wells containing 100 μL of assay buffer in duplicate, covered, and incubated on a plate shaker (approximately at 200 rpm) for 60 min at room temperature. The wells were washed 3 times with 300 μL of 1X wash buffer followed by the addition of 100 μL of Ab-enzyme conjugate into each well, mixed gently for 10 secs, covered, and incubated the plate on a plate shaker (approximately at 200 rpm) for 30 min at room temperature. The wells were then washed 3 times with 300 μL of 1X wash buffer followed by the addition of 100 μL of TMB substrate per well, mixed gently for 10 secs, cover and incubated the plate on a plate shaker (approximately at 200 rpm) at room temperature until the samples turned dark blue. The reaction was stopped by adding 50 μL of stopping solution to all wells and mixed gently. The absorbance was measured at 450 nm with SpectraMAX 190 (Molecular Devices).

Cell proliferation assay—LNCaP and 22Rv1 cells were plated in complete RPMI media (RPMI + penicillin (50 U/ml), streptomycin (50 U/ml), amphotericin B (50 U/ml), normocin (100 μg/ml), gentamicin (25 μg/ml) and 5% (V:V) FBS) at a density of 5000 cells per well of a 96-well plate. After 24 h, cells were washed and cultured in RPMI + 5% charcoal stripped FBS (csFBS) for an additional 24 h before dosing cells with the indicated concentration of test compounds in RPMI + 5% csFBS. After 1 h of incubation with the test compounds, culture media was spiked with 1 nM of R1881. Cells were allowed to incubate with the test compounds for a total of 24 h. Cell proliferation was determined using CellTiter 96® non-radioactive cell proliferation assay kit (Promega) and manufacturer's instructions.

GFP-tau assay—HEK293 cells stably carrying Dox-inducible GFP-tau (WT or P301L, 0N4R) were cultured in DMEM supplemented with 10% FBS and 1% P/S (Invitrogen). Cells were plated in 50 μL DMEM in 384-well plates (Greiner) coated with poly-D-lysine (Sigma). The next day, GFP-tau expression was induced by the addition of Dox (10 ng/mL). Compounds were then treated in 8-point dose starting at 20 μM in duplicate and incubated at 37°C for 24 h. 30 minutes before the end of the 24-h incubation, cells were treated with Hoechst 33342 at the final concentration of 0.5 μg/mL. High-throughput imaging at 20X was performed on an InCell6000 automated microscope (GE) and GFP intensity of each cell was quantify using the InCell Analyzer Workstation (GE). To quantify effects of compounds tested, the median value of GFP intensity per cell of each well was computed and normalized to the average median GFP intensity of all DMSO treated wells (32 wells in each

plate). Cell count of each well was measured and normalized to the average cell count of all DMSO treated wells. Wells with a normalized cell count lower than 0.65 were disregarded. Curve fitting of the dose curve was conducted by Prism 7 (GraphPad).

Western blot of tau—HeLa cells stably expressing tau (0N4R) were washed in ice-cold PBS and incubated with lysis buffer (50mM Tris-HCl, 150mM NaCl, 1% TritonX100, 2mg/ml protease inhibitor cocktail (Pierce)) on ice for 30 min with occasional mixing. Cell lysates were collected by scraping and centrifuged at 20 000xg for 20 min. The postnuclear supernatants were transferred to a new tube and the protein content determined by Bradford assay. Equal amounts of total protein were separated on a 12% SDS-PAGE and subsequently transferred to nitrocellulose, blocked with 5% skim milk solution (50mM Tris-HCl pH 7.4, 150mM NaCl and 0.5% Tween20) and probed with the indicated primary and HRP-linked secondary antibodies. The immunoblots were revealed with ECL.

Tau IP—For co-immunoprecipitation from HEK293 cells stably expressing Tau (0N4R), cells were washed with cold PBS and harvested in immunoprecipitation buffer (0.1% Triton X-100, 2 μg/ml aprotinin, 100 μg/ml PMSF, 100 mM NaCl in 50 mM Tris–HCl, pH 7.2). The lysate was sonicated, pre-cleared for 1 h at 4°C with 25 μl of protein G (Pierce) and centrifuged at 14 000 rpm. The supernatants were incubated with 2 μg of Tau antibody (Alz50) and 60 μl of protein G and rocked at 4°C overnight. The protein G beads we re pelleted and washed three times with immunoprecipitation buffer. The precipitates were resolved on SDS–PAGE gel and subjected to western blot analysis with the indicated antibody. Bands were visualized by chemiluminescence (Pierce).

Brain slice quantitation of pS396/S404 tau—The cerebellum and brainstem of 4-month old rTg4510 brain were removed and the hemispheres (cortex/hippocampus) were sectioned into 400 μm thick slices which were then separated in ice cold buffer. Slices were transferred to six well plates containing 0.4 μm pore membrane inserts. Sections from each hemibrain are plated in the same row, thus providing two complete hemispheres and allowing each mouse to serve as its own control. Slices were maintained in culture for 14 d in media containing 25% serum with media exchanged every 2 d. After the incubation period, each hemibrain was treated with SEW84 or DMSO, n = six mice per group. Following treatment, slices from each hemibrain were pooled together for analysis (Congdon et al., 2012).

QUANTIFICATION AND STATISTICAL ANALYSIS

Two tailed Student’s t-test was used to compare two groups using GraphPad Prism software. One-way ANOVA with post hoc Tukey’s HSD test was used to compare multiple groups using XLSTAT by Addinsoft. Sample size for each experiment is indicated in the figure legends.

DATA AND CODE AVAILABILITY

This study did not generate any unique datasets or code in repositories.

ADDITONAL RESOURCES

None.

Supplementary Material

Refer to Web version on PubMed Central for supplementary material.

Acknowledgements

Support was provided by the National Institutes of Health (NIH) Grants HL095524, DK051870 and AG049665 to WEB, R01NS059690 to J.E.G., GM057374 as well as GM113251 and GM131693 to H.J.D., R01GM043601 to D.F. and G12MD007590 & P20MD002285 to J.C.. M.B.C., J.C.S and N.C.G. were supported by NIH grant 2G12MD007592 to the Border Biomedical Research Center (BBRC), from the National Institutes on Minority Health and Health Disparities (NIMHD). M.B.C and J.C. are supported by the Lizanell and Colbert Coldwell Foundation and the Department of Defense (DOD) Prostate Cancer Research Program (PCRP) (W81XWH-17-1-0435). N.R.O. received support from RISE Scholars Program at UTEP (NIGMS grant R25GM069621-11).

References

ANTONARAKIS ES, LU C, WANG H, LUBER B, NAKAZAWA M, ROESER JC, CHEN Y, MOHAMMAD TA, CHEN Y, FEDOR HL, LOTAN TL, ZHENG Q, DE MARZO AM, ISAACS JT, ISAACS WB, NADAL R, PALLER CJ, DENMEADE SR, CARDUCCI MA, EISENBERGER MA & LUO J 2014 AR-V7 and resistance to enzalutamide and abiraterone in prostate cancer. N Engl J Med, 371, 1028–38. [PubMed: 25184630]

ARORA VK, SCHENKEIN E, MURALI R, SUBUDHI SK, WONGVIPAT J, BALBAS MD, SHAH N, CAI L, EFSTATHIOU E, LOGOTHETIS C, ZHENG D & SAWYERS CL 2013 Glucocorticoid receptor confers resistance to antiandrogens by bypassing androgen receptor blockade. Cell, 155, 1309–22. [PubMed: 24315100]

ATTARD G, REID AH, YAP TA, RAYNAUD F, DOWSETT M, SETTATREE S, BARRETT M, PARKER C, MARTINS V, FOLKERD E, CLARK J, COOPER CS, KAYE SB, DEARNALEY D, LEE G & DE BONO JS 2008 Phase I clinical trial of a selective inhibitor of CYP17, abiraterone acetate, confirms that castration-resistant prostate cancer commonly remains hormone driven. J Clin Oncol, 26, 4563–71. [PubMed: 18645193]

BAKER JD, OZSAN I, RODRIGUEZ OSPINA S, GULICK D & BLAIR LJ 2018 Hsp90 Heterocomplexes Regulate Steroid Hormone Receptors: From Stress Response to Psychiatric Disease. Int J Mol Sci, 20.

BALCH WE, MORIMOTO RI, DILLIN A & KELLY JW 2008 Adapting proteostasis for disease intervention. Science, 319, 916–9. [PubMed: 18276881]

BALCHIN D, HAYER-HARTL M & HARTL FU 2016 In vivo aspects of protein folding and quality control. Science, 353, aac4354. [PubMed: 27365453]

BOSELLI M, LEE BH, ROBERT J, PRADO MA, MIN SW, CHENG C, SILVA MC, SEONG C, ELSASSER S, HATLE KM, GAHMAN TC, GYGI SP, HAGGARTY SJ, GAN L, KING RW & FINLEY D 2017 An inhibitor of the proteasomal deubiquitinating enzyme USP14 induces tau elimination in cultured neurons. J Biol Chem, 292, 19209–19225. [PubMed: 28972160]

CHADLI A, FELTS SJ, WANG Q, SULLIVAN WP, BOTUYAN MV, FAUQ A, RAMIREZ-ALVARADO M & MER G 2010 Celastrol inhibits Hsp90 chaperoning of steroid receptors by inducing fibrillization of the Co-chaperone p23. J Biol Chem, 285, 4224–31. [PubMed: 19996313]

CHANG L, BERTELSEN EB, WISEN S, LARSEN EM, ZUIDERWEG ER & GESTWICKI JE 2008 High-throughput screen for small molecules that modulate the ATPase activity of the molecular chaperone DnaK. Anal Biochem, 372, 167–76. [PubMed: 17904512]

COHEN SM, MUKERJI R, SAMADI AK, ZHANG X, ZHAO H, BLAGG BS & COHEN MS 2012 Novel C-terminal Hsp90 inhibitor for head and neck squamous cell cancer (HNSCC) with in vivo efficacy and improved toxicity profiles compared with standard agents. Ann Surg Oncol, 19 Suppl 3, S483–90. [PubMed: 21837531]

COPPINGER JA, HUTT DM, RAZVI A, KOULOV AV, PANKOW S, YATES JR 3RD & BALCH WE 2012 A chaperone trap contributes to the onset of cystic fibrosis. PLoS One, 7, e37682. [PubMed: 22701530]

DE LEON JT, IWAI A, FEAU C, GARCIA Y, BALSIGER HA, STORER CL, SURO RM, GARZA KM, LEE S, KIM YS, CHEN Y, NING YM, RIGGS DL, FLETTERICK RJ, GUY RK, TREPEL JB, NECKERS LM & COX MB 2011 Targeting the regulation of androgen receptor signaling by the heat shock protein 90 cochaperone FKBP52 in prostate cancer cells. Proc Natl Acad Sci U S A, 108, 11878–83. [PubMed: 21730179]

DICKEY CA, DUNMORE J, LU B, WANG JW, LEE WC, KAMAL A, BURROWS F, ECKMAN C, HUTTON M & PETRUCELLI L 2006 HSP induction mediates selective clearance of tau phosphorylated at proline-directed Ser/Thr sites but not KXGS (MARK) sites. FASEB J, 20, 753–5. [PubMed: 16464956]

DICKEY CA, KAMAL A, LUNDGREN K, KLOSAK N, BAILEY RM, DUNMORE J, ASH P, SHORAKA S, ZLATKOVIC J, ECKMAN CB, PATTERSON C, DICKSON DW, NAHMAN NS JR., HUTTON M, BURROWS F & PETRUCELLI L 2007 The high-affinity HSP90-CHIP complex recognizes and selectively degrades phosphorylated tau client proteins. J Clin Invest, 117, 648–58. [PubMed: 17304350]

DRUBIN DG & KIRSCHNER MW 1986 Tau protein function in living cells. J Cell Biol, 103, 2739–46. [PubMed: 3098742]

ECHEVERRIA PC, BERNTHALER A, DUPUIS P, MAYER B & PICARD D 2011 An interaction network predicted from public data as a discovery tool: application to the Hsp90 molecular chaperone machine. PLoS One, 6, e26044. [PubMed: 22022502]

ELO JP, KVIST L, LEINONEN K, ISOMAA V, HENTTU P, LUKKARINEN O & VIHKO P 1995 Mutated human androgen receptor gene detected in a prostatic cancer patient is also activated by estradiol. J Clin Endocrinol Metab, 80, 3494–500. [PubMed: 8530589]

GELLER R, PECHMANN S, ACEVEDO A, ANDINO R & FRYDMAN J 2018 Hsp90 shapes protein and RNA evolution to balance trade-offs between protein stability and aggregation. Nat Commun, 9, 1781. [PubMed: 29725062]

GILLIS JL, SELTH LA, CENTENERA MM, TOWNLEY SL, SUN S, PLYMATE SR, TILLEY WD & BUTLER LM 2013 Constitutively-active androgen receptor variants function independently of the HSP90 chaperone but do not confer resistance to HSP90 inhibitors. Oncotarget, 4, 691–704. [PubMed: 23674566]

GLAZE ER, LAMBERT AL, SMITH AC, PAGE JG, JOHNSON WD, MCCORMICK DL, BROWN AP, LEVINE BS, COVEY JM, EGORIN MJ, EISEMAN JL, HOLLERAN JL, SAUSVILLE EA & TOMASZEWSKI JE 2005 Preclinical toxicity of a geldanamycin analog, 17-(dimethylaminoethylamino)-17-demethoxygeldanamycin (17-DMAG), in rats and dogs: potential clinical relevance. Cancer Chemother Pharmacol, 56, 637–47. [PubMed: 15986212]

GRAF C, STANKIEWICZ M, KRAMER G & MAYER MP 2009 Spatially and kinetically resolved changes in the conformational dynamics of the Hsp90 chaperone machine. EMBO J, 28, 602–13. [PubMed: 19165152]

GRIGORYEV DN, LONG BJ, NJAR VC & BRODIE AH 2000 Pregnenolone stimulates LNCaP prostate cancer cell growth via the mutated androgen receptor. J Steroid Biochem Mol Biol, 75, 1–10. [PubMed: 11179903]

GUPTA R, KASTURI P, BRACHER A, LOEW C, ZHENG M, VILLELLA A, GARZA D, HARTL FU & RAYCHAUDHURI S 2011 Firefly luciferase mutants as sensors of proteome stress. Nat Methods, 8, 879–84. [PubMed: 21892152]

GUTHRIE CR & KRAEMER BC 2011 Proteasome inhibition drives HDAC6-dependent recruitment of tau to aggresomes. J Mol Neurosci, 45, 32–41. [PubMed: 21340680]

HALL JA, SEEDARALA S, ZHAO H, GARG G, GHOSH S & BLAGG BS 2016 Novobiocin Analogues That Inhibit the MAPK Pathway. J Med Chem, 59, 925–33. [PubMed: 26745854]

HARST A, LIN H & OBERMANN WM 2005 Aha1 competes with Hop, p50 and p23 for binding to the molecular chaperone Hsp90 and contributes to kinase and hormone receptor activation. Biochem J, 387, 789–96. [PubMed: 15584899]

HASEGAWA M, SMITH MJ & GOEDERT M 1998 Tau proteins with FTDP-17 mutations have a reduced ability to promote microtubule assembly. FEBS Lett, 437, 207–10. [PubMed: 9824291]

HONG M, ZHUKAREVA V, VOGELSBERG-RAGAGLIA V, WSZOLEK Z, REED L, MILLER BI, GESCHWIND DH, BIRD TD, MCKEEL D, GOATE A, MORRIS JC, WILHELMSEN KC, SCHELLENBERG GD, TROJANOWSKI JQ & LEE VM 1998 Mutation-specific functional impairments in distinct tau isoforms of hereditary FTDP-17. Science, 282, 1914–7. [PubMed: 9836646]

HORVAT NK, ARMSTRONG H, LEE BL, MERCIER R, WOLMARANS A, KNOWLES J, SPYRACOPOULOS L & LAPOINTE P 2014 A mutation in the catalytic loop of Hsp90 specifically impairs ATPase stimulation by Aha1p, but not Hch1p. J Mol Biol, 426, 2379–92. [PubMed: 24726918]

IHRIG V & OBERMANN WMJ 2017 Identifying Inhibitors of the Hsp90-Aha1 Protein Complex, a Potential Target to Drug Cystic Fibrosis, by Alpha Technology. SLAS Discov, 22, 923–928. [PubMed: 28346090]

IYER G, MORRIS MJ, RATHKOPF D, SLOVIN SF, STEERS M, LARSON SM, SCHWARTZ LH, CURLEY T, DELACRUZ A, YE Q, HELLER G, EGORIN MJ, IVY SP, ROSEN N, SCHER HI & SOLIT DB 2012 A phase I trial of docetaxel and pulse-dose 17-allylamino-17-demethoxygeldanamycin in adult patients with solid tumors. Cancer Chemother Pharmacol, 69, 1089–97. [PubMed: 22124669]

JINWAL UK, MIYATA Y, KOREN J 3RD, JONES JR, TROTTER JH, CHANG L, O'LEARY J, MORGAN D, LEE DC, SHULTS CL, ROUSAKI A, WEEBER EJ, ZUIDERWEG ER, GESTWICKI JE & DICKEY CA 2009 Chemical manipulation of hsp70 ATPase activity regulates tau stability. J Neurosci, 29, 12079–88. [PubMed: 19793966]

JOSHI S, WANG T, ARAUJO TLS, SHARMA S, BRODSKY JL & CHIOSIS G 2018 Adapting to stress - chaperome networks in cancer. Nat Rev Cancer, 18, 562–575. [PubMed: 29795326]

KARAGOZ GE, DUARTE AM, AKOURY E, IPPEL H, BIERNAT J, MORAN LUENGO T, RADLI M, DIDENKO T, NORDHUES BA, VEPRINTSEV DB, DICKEY CA, MANDELKOW E, ZWECKSTETTER M, BOELENS R, MADL T & RUDIGER SG 2014 Hsp90-Tau complex reveals molecular basis for specificity in chaperone action. Cell, 156, 963–74. [PubMed: 24581495]

KARRAS GI, YI S, SAHNI N, FISCHER M, XIE J, VIDAL M, D'ANDREA AD, WHITESELL L & LINDQUIST S 2017 HSP90 Shapes the Consequences of Human Genetic Variation. Cell, 168, 856–866 e12. [PubMed: 28215707]

KINOSHITA E, KINOSHITA-KIKUTA E & KOIKE T 2009 Separation and detection of large phosphoproteins using Phos-tag SDS-PAGE. Nat Protoc, 4, 1513–21. [PubMed: 19798084]

KINOSHITA E, KINOSHITA-KIKUTA E, SHIBA A, EDAHIRO K, INOUE Y, YAMAMOTO K, YOSHIDA M & KOIKE T 2014 Profiling of protein thiophosphorylation by Phos-tag affinity electrophoresis: evaluation of adenosine 5'-O-(3-thiotriphosphate) as a phosphoryl donor in protein kinase reactions. Proteomics, 14, 668–79. [PubMed: 24453221]

KISHINEVSKY S, WANG T, RODINA A, CHUNG SY, XU C, PHILIP J, TALDONE T, JOSHI S, ALPAUGH ML, BOLAENDER A, GUTBIER S, SANDHU D, FATTAHI F, ZIMMER B, SHAH SK, CHANG E, INDA C, KOREN J 3RD, SAURAT NG, LEIST M, GROSS SS, SESHAN VE, KLEIN C, TOMISHIMA MJ, ERDJUMENT-BROMAGE H, NEUBERT TA, HENRICKSON RC, CHIOSIS G & STUDER L 2018 HSP90-incorporating chaperome networks as biosensor for disease-related pathways in patient-specific midbrain dopamine neurons. Nat Commun, 9, 4345. [PubMed: 30341316]

KOULOV AV, LAPOINTE P, LU B, RAZVI A, COPPINGER J, DONG MQ, MATTESON J, LAISTER R, ARROWSMITH C, YATES JR 3RD & BALCH WE 2010 Biological and structural basis for Aha1 regulation of Hsp90 ATPase activity in maintaining proteostasis in the human disease cystic fibrosis. Mol Biol Cell, 21, 871–84. [PubMed: 20089831]

KUSUMA BR, ZHANG L, SUNDSTROM T, PETERSON LB, DOBROWSKY RT & BLAGG BS 2012 Synthesis and evaluation of novologues as C-terminal Hsp90 inhibitors with cytoprotective activity against sensory neuron glucotoxicity. J Med Chem, 55, 5797–812. [PubMed: 22702513]

LEPVRIER E, MOULLINTRAFFORT L, NIGEN M, GOUDE R, ALLEGRO D, BARBIER P, PEYROT V, THOMAS D, NAZABAL A & GARNIER C 2015 Hsp90 Oligomers Interacting with

the Aha1 Cochaperone: An Outlook for the Hsp90 Chaperone Machineries. Anal Chem, 87, 7043–51. [PubMed: 26076190]

LI J, RICHTER K, REINSTEIN J & BUCHNER J 2013a Integration of the accelerator Aha1 in the Hsp90 co-chaperone cycle. Nat Struct Mol Biol, 20, 326–31. [PubMed: 23396352]

LI J, SOROKA J & BUCHNER J 2012 The Hsp90 chaperone machinery: conformational dynamics and regulation by co-chaperones. Biochim Biophys Acta, 1823, 624–35. [PubMed: 21951723]

LI X, SRINIVASAN SR, CONNARN J, AHMAD A, YOUNG ZT, KABZA AM, ZUIDERWEG ER, SUN D & GESTWICKI JE 2013b Analogs of the Allosteric Heat Shock Protein 70 (Hsp70) Inhibitor, MKT-077, as Anti-Cancer Agents. ACS Med Chem Lett, 4.

LUO W, DOU F, RODINA A, CHIP S, KIM J, ZHAO Q, MOULICK K, AGUIRRE J, WU N, GREENGARD P & CHIOSIS G 2007 Roles of heat-shock protein 90 in maintaining and facilitating the neurodegenerative phenotype in tauopathies. Proc Natl Acad Sci U S A, 104, 9511–6. [PubMed: 17517623]

MCLAUGHLIN SH, VENTOURAS LA, LOBBEZOO B & JACKSON SE 2004 Independent ATPase activity of Hsp90 subunits creates a flexible assembly platform. J Mol Biol, 344, 813–26. [PubMed: 15533447]

MEYER P, PRODROMOU C, LIAO C, HU B, ROE SM, VAUGHAN CK, VLASIC I, PANARETOU B, PIPER PW & PEARL LH 2004 Structural basis for recruitment of the ATPase activator Aha1 to the Hsp90 chaperone machinery. EMBO J, 23, 1402–10. [PubMed: 15039704]

MIYAMOTO H, YEH S, WILDING G & CHANG C 1998 Promotion of agonist activity of antiandrogens by the androgen receptor coactivator, ARA70, in human prostate cancer DU145 cells. Proc Natl Acad Sci U S A, 95, 7379–84. [PubMed: 9636157]

MOK SA, CONDELLO C, FREILICH R, GILLIES A, ARHAR T, OROZ J, KADAVATH H, JULIEN O, ASSIMON VA, RAUCH JN, DUNYAK BM, LEE J, TSAI FTF, WILSON MR, ZWECKSTETTER M, DICKEY CA & GESTWICKI JE 2018 Mapping interactions with the chaperone network reveals factors that protect against tau aggregation. Nat Struct Mol Biol, 25, 384–393. [PubMed: 29728653]

MORAN LUENGO T, KITYK R, MAYER MP & RUDIGER SGD 2018 Hsp90 Breaks the Deadlock of the Hsp70 Chaperone System. Mol Cell, 70, 545–552 e9. [PubMed: 29706537]

MOSES MA, KIM YS, RIVERA-MARQUEZ GM, OSHIMA N, WATSON MJ, BEEBE KE, WELLS C, LEE S, ZUEHLKE AD, SHAO H, BINGMAN WE 3RD, KUMAR V, MALHOTRA SV, WEIGEL NL, GESTWICKI JE, TREPEL JB & NECKERS LM 2018 Targeting the Hsp40/Hsp70 Chaperone Axis as a Novel Strategy to Treat Castration-Resistant Prostate Cancer. Cancer Res, 78, 4022–4035. [PubMed: 29764864]

PRATT WB & DITTMAR KD 1998 Studies with Purified Chaperones Advance the Understanding of the Mechanism of Glucocorticoid Receptor-hsp90 Heterocomplex Assembly. Trends Endocrinol Metab, 9, 244–52. [PubMed: 18406276]

PRATT WB, GESTWICKI JE, OSAWA Y & LIEBERMAN AP 2015 Targeting Hsp90/Hsp70-based protein quality control for treatment of adult onset neurodegenerative diseases. Annu Rev Pharmacol Toxicol, 55, 353–71. [PubMed: 25292434]

QUEITSCH C, SANGSTER TA & LINDQUIST S 2002 Hsp90 as a capacitor of phenotypic variation. Nature, 417, 618–24. [PubMed: 12050657]

REHN AB & BUCHNER J 2015 p23 and Aha1. Subcell Biochem, 78, 113–31. [PubMed: 25487019]

RETZLAFF M, HAGN F, MITSCHKE L, HESSLING M, GUGEL F, KESSLER H, RICHTER K & BUCHNER J 2010 Asymmetric activation of the hsp90 dimer by its cochaperone aha1. Mol Cell, 37, 344–54. [PubMed: 20159554]

RETZLAFF M, STAHL M, EBERL HC, LAGLEDER S, BECK J, KESSLER H & BUCHNER J 2009 Hsp90 is regulated by a switch point in the C-terminal domain. EMBO Rep, 10, 1147–53. [PubMed: 19696785]

RODINA A, WANG T, YAN P, GOMES ED, DUNPHY MP, PILLARSETTY N, KOREN J, GERECITANO JF, TALDONE T, ZONG H, CALDAS-LOPES E, ALPAUGH M, CORBEN A, RIOLO M, BEATTIE B, PRESSL C, PETER RI, XU C, TRONDL R, PATEL HJ, SHIMIZU F, BOLAENDER A, YANG C, PANCHAL P, FAROOQ MF, KISHINEVSKY S, MODI S, LIN O, CHU F, PATIL S, ERDJUMENT-BROMAGE H, ZANZONICO P, HUDIS C, STUDER L,

ROBOZ GJ, CESARMAN E, CERCHIETTI L, LEVINE R, MELNICK A, LARSON SM, LEWIS JS, GUZMAN ML & CHIOSIS G 2016 The epichaperome is an integrated chaperome network that facilitates tumour survival. Nature, 538, 397–401. [PubMed: 27706135]

ROE SM, PRODROMOU C, O'BRIEN R, LADBURY JE, PIPER PW & PEARL LH 1999 Structural basis for inhibition of the Hsp90 molecular chaperone by the antitumor antibiotics radicicol and geldanamycin. J Med Chem, 42, 260–6. [PubMed: 9925731]

SAHASRABUDHE P, ROHRBERG J, BIEBL MM, RUTZ DA & BUCHNER J 2017 The Plasticity of the Hsp90 Co-chaperone System. Mol Cell, 67, 947–961 e5. [PubMed: 28890336]

SAHU B, LAAKSO M, PIHLAJAMAA P, OVASKA K, SINIELNIKOV I, HAUTANIEMI S & JANNE OA 2013 FoxA1 specifies unique androgen and glucocorticoid receptor binding events in prostate cancer cells. Cancer Res, 73, 1570–80. [PubMed: 23269278]

SALA AJ, BOTT LC & MORIMOTO RI 2017 Shaping proteostasis at the cellular, tissue, and organismal level. J Cell Biol, 216, 1231–1241. [PubMed: 28400444]

SAMADI AK, ZHANG X, MUKERJI R, DONNELLY AC, BLAGG BS & COHEN MS 2011 A novel C-terminal HSP90 inhibitor KU135 induces apoptosis and cell cycle arrest in melanoma cells. Cancer Lett, 312, 158–67. [PubMed: 21924824]

SCHOPF FH, BIEBL MM & BUCHNER J 2017 The HSP90 chaperone machinery. Nat Rev Mol Cell Biol, 18, 345–360. [PubMed: 28429788]

SCHULTE TW, AKINAGA S, SOGA S, SULLIVAN W, STENSGARD B, TOFT D & NECKERS LM 1998 Antibiotic radicicol binds to the N-terminal domain of Hsp90 and shares important biologic activities with geldanamycin. Cell Stress Chaperones, 3, 100–8. [PubMed: 9672245]

SHAFI AA, COX MB & WEIGEL NL 2013 Androgen receptor splice variants are resistant to inhibitors of Hsp90 and FKBP52, which alter androgen receptor activity and expression. Steroids, 78, 548–54. [PubMed: 23380368]

SHELTON LB, BAKER JD, ZHENG D, SULLIVAN LE, SOLANKI PK, WEBSTER JM, SUN Z, SABBAGH JJ, NORDHUES BA, KOREN J 3RD, GHOSH S, BLAGG BSJ, BLAIR LJ & DICKEY CA 2017 Hsp90 activator Aha1 drives production of pathological tau aggregates. Proc Natl Acad Sci U S A, 114, 9707–9712. [PubMed: 28827321]

SINGH JK, MAKDE RD, KUMAR V & PANDA D 2007 A membrane protein, EzrA, regulates assembly dynamics of FtsZ by interacting with the C-terminal tail of FtsZ. Biochemistry, 46, 11013–22. [PubMed: 17718511]

SREERAMULU S, GANDE SL, GOBEL M & SCHWALBE H 2009 Molecular mechanism of inhibition of the human protein complex Hsp90-Cdc37, a kinome chaperone-cochaperone, by triterpene celastrol. Angew Chem Int Ed Engl, 48, 5853–5. [PubMed: 19585625]

STIEGLER SC, RUBBELKE M, KOROTKOV VS, WEIWAD M, JOHN C, FISCHER G, SIEBER SA, SATTLER M & BUCHNER J 2017 A chemical compound inhibiting the Aha1-Hsp90 chaperone complex. J Biol Chem, 292, 17073–17083. [PubMed: 28851842]

SYNORADZKI K & BIEGANOWSKI P 2015 Middle domain of human Hsp90 isoforms differentially binds Aha1 in human cells and alters Hsp90 activity in yeast. Biochim Biophys Acta, 1853, 445–52. [PubMed: 25486457]

TAIPALE M, JAROSZ DF & LINDQUIST S 2010 HSP90 at the hub of protein homeostasis: emerging mechanistic insights. Nat Rev Mol Cell Biol, 11, 515–28. [PubMed: 20531426]

TAN J, SHARIEF Y, HAMIL KG, GREGORY CW, ZANG DY, SAR M, GUMERLOCK PH, DEVERE WHITE RW, PRETLOW TG, HARRIS SE, WILSON EM, MOHLER JL & FRENCH FS 1997 Dehydroepiandrosterone activates mutant androgen receptors expressed in the androgen-dependent human prostate cancer xenograft CWR22 and LNCaP cells. Mol Endocrinol, 11, 450–9. [PubMed: 9092797]

TRAN C, OUK S, CLEGG NJ, CHEN Y, WATSON PA, ARORA V, WONGVIPAT J, SMITH-JONES PM, YOO D, KWON A, WASIELEWSKA T, WELSBIE D, CHEN CD, HIGANO CS, BEER TM, HUNG DT, SCHER HI, JUNG ME & SAWYERS CL 2009 Development of a second-generation antiandrogen for treatment of advanced prostate cancer. Science, 324, 787–90. [PubMed: 19359544]

TRIPATHI V, DARNAUER S, HARTWIG NR & OBERMANN WM 2014 Aha1 can act as an autonomous chaperone to prevent aggregation of stressed proteins. J Biol Chem, 289, 36220–8. [PubMed: 25378400]

VERBA KA & AGARD DA 2017 How Hsp90 and Cdc37 Lubricate Kinase Molecular Switches. Trends Biochem Sci, 42, 799–811. [PubMed: 28784328]

VON BERGEN M, FRIEDHOFF P, BIERNAT J, HEBERLE J, MANDELKOW EM & MANDELKOW E 2000 Assembly of tau protein into Alzheimer paired helical filaments depends on a local sequence motif ((306)VQIVYK(311)) forming beta structure. Proc Natl Acad Sci U S A, 97, 5129–34. [PubMed: 10805776]

WANG C & BALCH WE 2018 Bridging Genomics to Phenomics at Atomic Resolution through Variation Spatial Profiling. Cell Rep, 24, 2013–2028 e6. [PubMed: 30134164]

WANG H, LU M, YAO M & ZHU W 2016 Effects of treatment with an Hsp90 inhibitor in tumors based on 15 phase II clinical trials. Mol Clin Oncol, 5, 326–334. [PubMed: 27602225]

WANG X, VENABLE J, LAPOINTE P, HUTT DM, KOULOV AV, COPPINGER J, GURKAN C, KELLNER W, MATTESON J, PLUTNER H, RIORDAN JR, KELLY JW, YATES JR 3RD & BALCH WE 2006 Hsp90 cochaperone Aha1 downregulation rescues misfolding of CFTR in cystic fibrosis. Cell, 127, 803–15. [PubMed: 17110338]

WOLMARANS A, LEE B, SPYRACOPOULOS L & LAPOINTE P 2016 The Mechanism of Hsp90 ATPase Stimulation by Aha1. Sci Rep, 6, 33179. [PubMed: 27615124]

WORTMANN P, GOTZ M & HUGEL T 2017 Cooperative Nucleotide Binding in Hsp90 and Its Regulation by Aha1. Biophys J, 113, 1711–1718. [PubMed: 29045865]

YOUNG ZT, MOK SA & GESTWICKI JE 2018 Therapeutic Strategies for Restoring Tau Homeostasis. Cold Spring Harb Perspect Med, 8.

ZHANG JH, CHUNG TD & OLDENBURG KR 1999 A Simple Statistical Parameter for Use in Evaluation and Validation of High Throughput Screening Assays. J Biomol Screen, 4, 67–73. [PubMed: 10838414]

ZHANG L, ZHAO H, BLAGG BS & DOBROWSKY RT 2012 C-terminal heat shock protein 90 inhibitor decreases hyperglycemia-induced oxidative stress and improves mitochondrial bioenergetics in sensory neurons. J Proteome Res, 11, 2581–93. [PubMed: 22413817]

ZHANG Z, YOU Z, DOBROWSKY RT & BLAGG BSJ 2018 Synthesis and evaluation of a ring-constrained Hsp90 C-terminal inhibitor that exhibits neuroprotective activity. Bioorg Med Chem Lett.

ZHAO H & BLAGG BS 2013 Novobiocin analogues with second-generation noviose surrogates. Bioorg Med Chem Lett, 23, 552–7. [PubMed: 23234644]

ZUCK P, O'DONNELL GT, CASSADAY J, CHASE P, HODDER P, STRULOVICI B & FERRER M 2005 Miniaturization of absorbance assays using the fluorescent properties of white microplates. Anal Biochem, 342, 254–9. [PubMed: 15949786]

Significance

Hsp90 has been the subject of numerous drug development efforts for the treatment of many human diseases ranging from neurodegeneration to cancer, yet to date all clinical trials have failed due to toxicity associated with broad spectrum Hsp90 inhibitors (Glaze et al., 2005, Wang et al., 2016). This toxicity likely stems from the fact that Hsp90 is an essential component of the protein folding machinery (Geller et al., 2018, Karras et al., 2017, Queitsch et al., 2002, Sahasrabudhe et al., 2017, Schopf et al., 2017) and a complete abrogation of its activity is deleterious to the function of all cells in the body. Herein we describe the identification of a novel small molecule inhibitor of the Aha1-stimulate Hsp90 ATPase activity, SEW84. The novelty of this small molecule inhibitor stems from the fact that it modulates the activity of Hsp90 by binding to the carboxy terminal domain of the Hsp90 co-chaperone, Aha1, thereby preventing it from bringing the 2 Hsp90 protomers into close apposition, a required step for activation of this molecular chaperones ATPase activity. In addition, we show that SEW84 does not target the basal chaperoning activity of Hsp90, thereby avoiding the toxic effects of Hsp90 targeting small molecules. We provide evidence that SEW84 is able to reduce the activity of a number of Hsp90-dependent disease associated proteins. This includes prostate cancer associated variants of the androgen receptor as well as aggregation prone variants of Tau, which are linked to a number of tauopathies, including Alzheimer's Disease. These data highlight the therapeutic potential of SEW84 and other similar co-chaperone targeting chaperones which limit the pool of affected client proteins thereby mitigating the toxic issues plaguing earlier Hsp90 inhibitors.

Highlights

- HTS identifies SEW84, a novel inhibitor of the Aha1-stimulate Hsp90 ATPase activity
- SEW84 does not affect the basal ATPase activity of Hsp90
- SEW84 reduces the expression and trophic activity of PCa linked AR variants
- SEW84 specifically clears phosphorylated tau

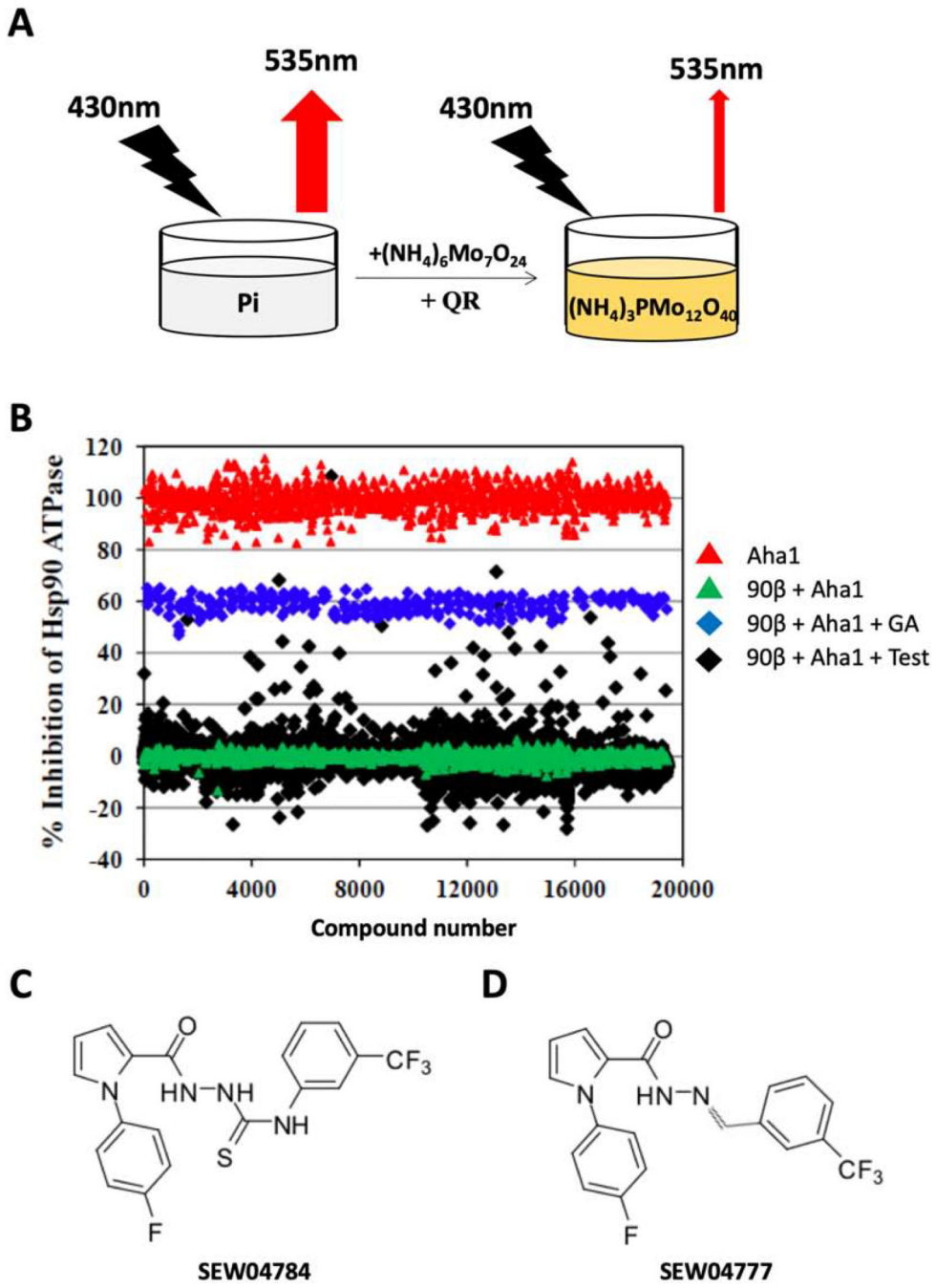

Figure 1. Identification of inhibitors of ASH activity.

A. Schema showing that inorganic phosphate (P_i) from the Hsp90-mediated hydrolysis of ATP, complexes with molybdate ($(NH_4)_6Mo_7O_{24}$) to form phosphomolybdate ($(NH_4)_3PMo_{12}O_{40}$) that can then bind to the quinaldine red (QR) dye to form a colored product that quenches the inherent fluorescence of the white microtiter plates. **B.** Scatterplot of the HTS to identify inhibitors of the ASH activity. The data are shown as a percent inhibition of the ASH activity, where Hsp90+Aha1 is set as 0% inhibition (green triangles)

and Aha1 is set as 100% inhibition (red triangles). Chemical structure of SEW84 (**C**) and SEW77 (**D**).

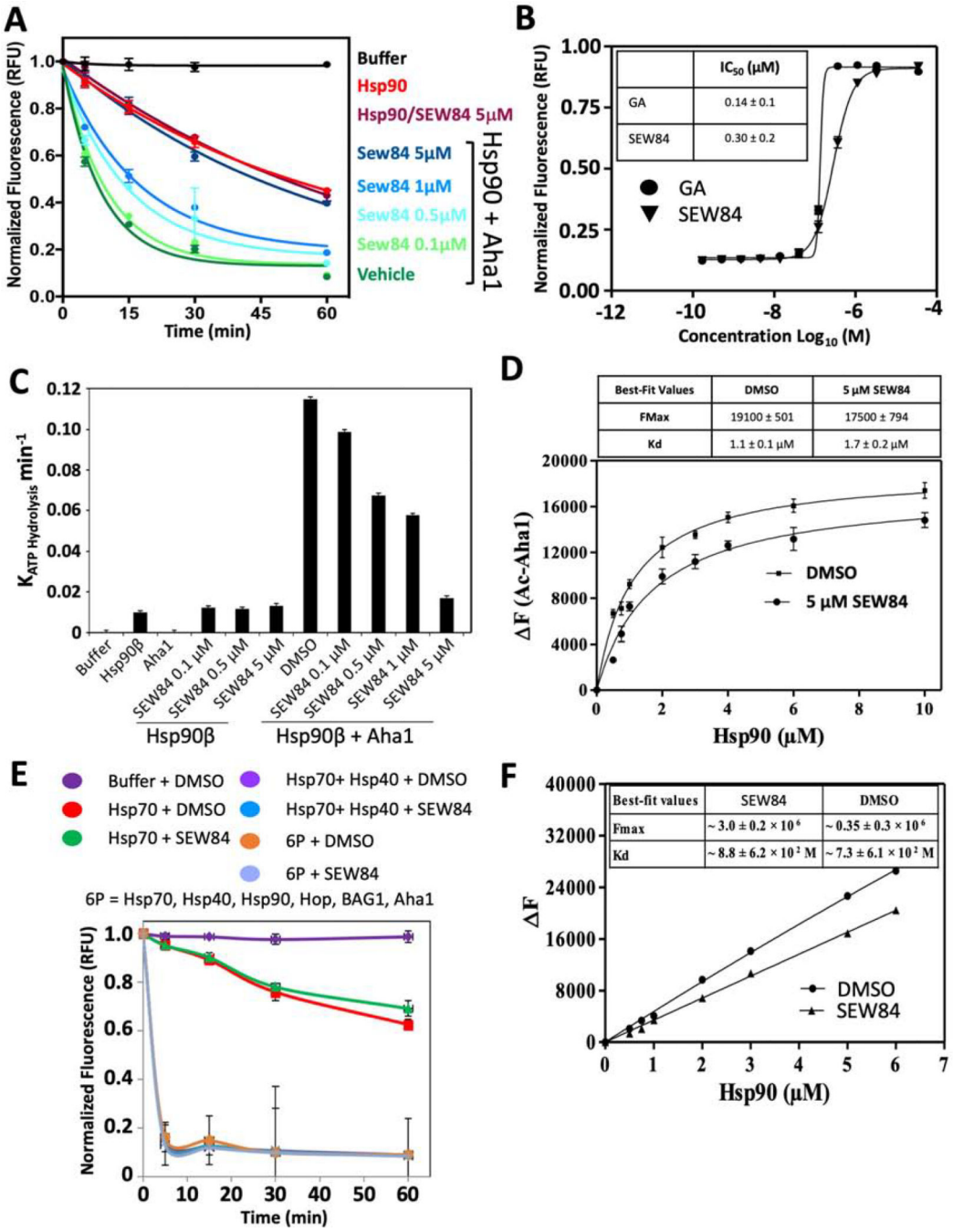

Figure 2. SEW84 specifically inhibits the ASH Activity

A. Scatter plot of the normalized fluorescence of the ASH assay over time in the presence of the indicated concentration of SEW84 **B.** Scatter plot of the normalized fluorescence of the ASH assay in the presence of GA (circles) and SEW84 (triangles). Inset Table depicts the IC_{50} values for GA and SEW84. **C.** Bar graph depicting the rate of the Hsp90 ATPase in the presence of Aha1 and the indicated dose of SEW84. **D.** Plot depicting the impact of increasing concentration of Hsp90β on the fluorescence of acrylodan-labeled full length Aha1 in the presence or absence of SEW84. The inset Table shows the Kd and Fmax. **E.** Plot

of the normalized fluorescence from QR reagent-based fluorescence quenching monitoring the impact of SEW84 on the ATPase activity of Hsp70 alone, in the presence of Hsp40 and in the context of the chaperone complex containing Hsp40, Hsp90, Hop, BAG1 and Aha1 (6P). **F.** Plot of the tryptophan fluorescence of Hsp90 in the presence or absence of 25 μM SEW84. The inset Table depicts the Fmax and Kd values. In all panels the error bars and values represent standard deviations ($n \geq 3$).

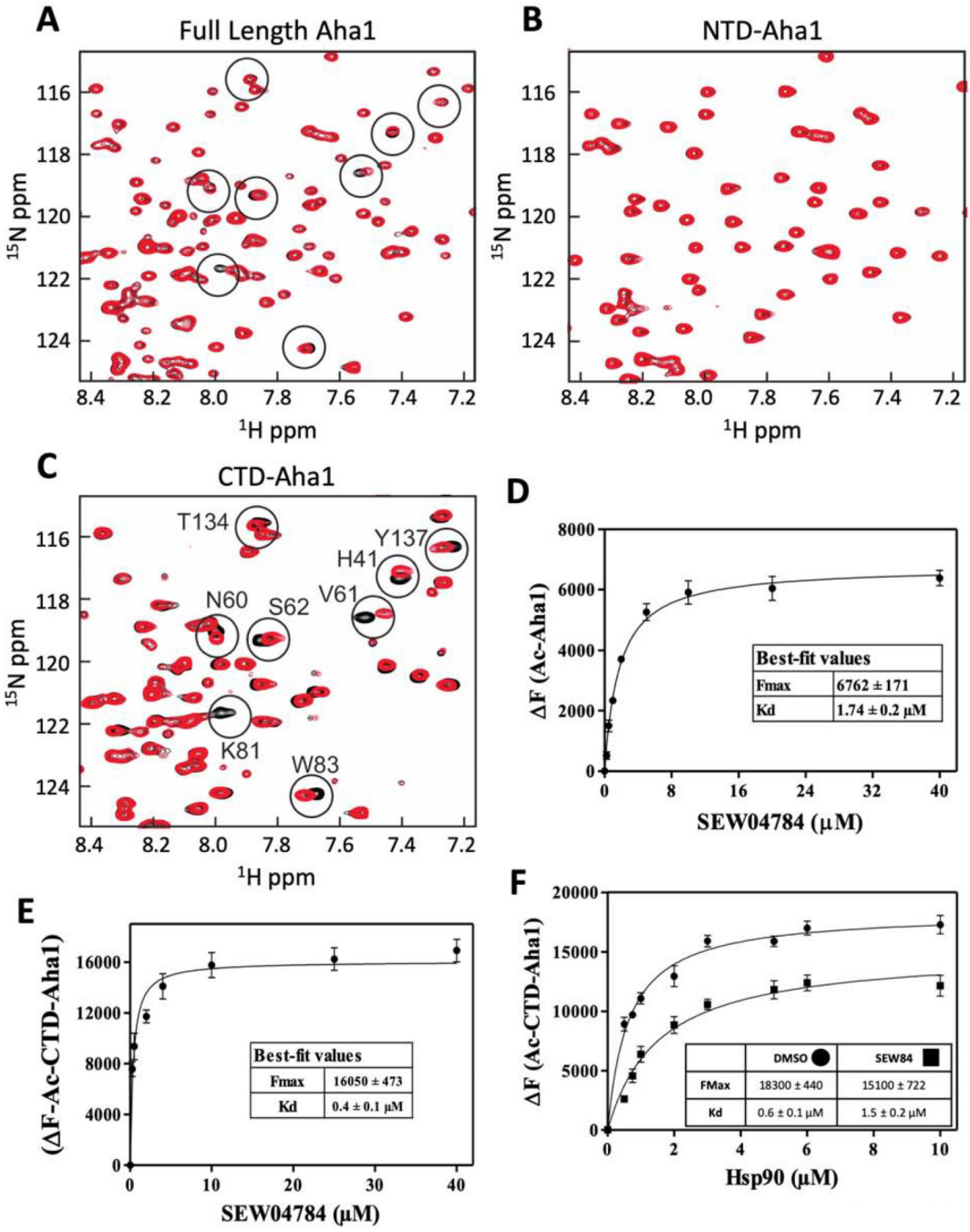

Figure 3. SEW84 binds to the C-terminal domain of Aha1.

A. Portions of superimposed 900 MHz ^{1}H-^{15}N-TROSY-HSQC spectra of full-length Aha1 in the presence of DMSO (black) or 100 μM SEW84 (red). Circles indicate differences in cross peak position. **B.** Overlay of 900 MHz ^{1}H-^{15}N-TROSY-HSQC spectra of the N-terminal domain of Aha1 in the presence of DMSO (black) or 100 μM SEW84 (blue). **C.** Overlay of 900 MHz ^{1}H-^{15}N-TROSY-HSQC spectra of the C-terminal domain of Aha1 in the presence of DMSO (black) or 100 μM SEW84 (blue). Assignments are shown and red circles indicate differences in cross peak position. Plot of the impact of SEW84 on the

fluorescence of acrylodan-labeled full length Aha1 (**D**) (ac-Aha1) and CTD-acAha1 (**E**). The inset tables depict the Fmax and Kd values. **F.** Plot depicting the impact of Hsp90β on the fluorescence of the acrylodan-labeled CTD-acAha1 in the presence or absence of 25 μM SEW84. The inset Table depicts the Kd and Fmax values. In all panels the error bars and values represent standard deviations ($n \geq 3$).

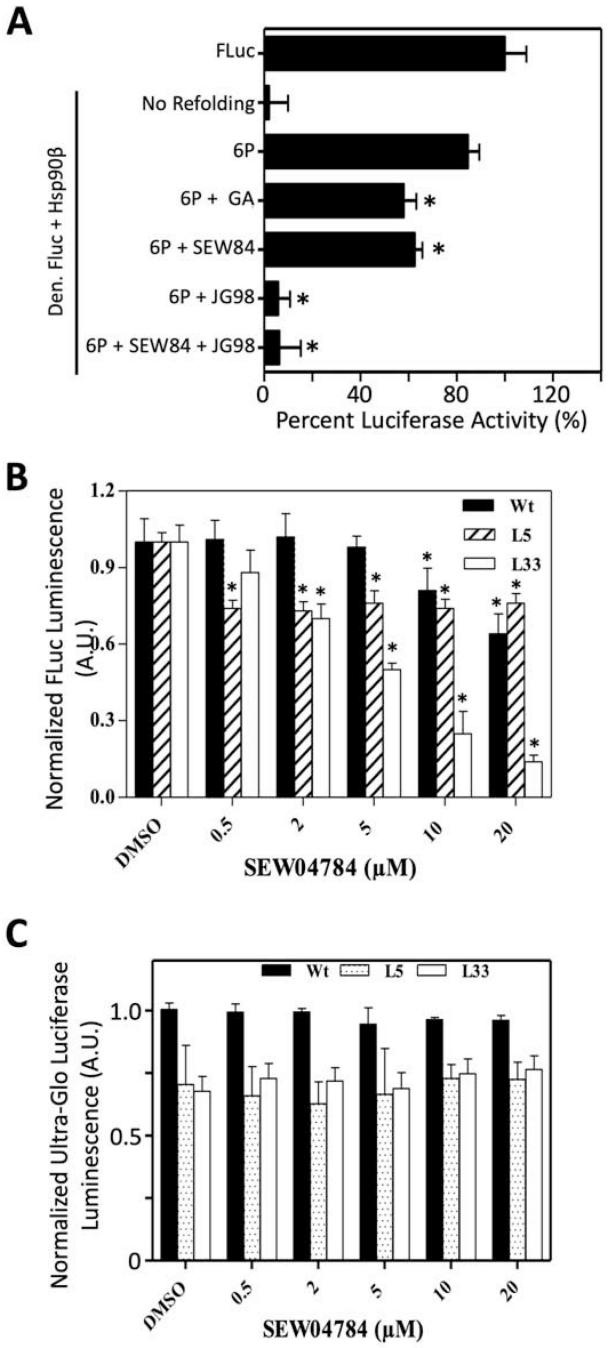

Figure 4. SEW84 inhibits the Hsp90-dependent folding of Firefly Luciferase.

A. Bar graph showing the normalized activity of Firefly Luciferase (FLuc) in response to *in vitro* refolding in the presence of the indicated chaperone proteins following heat denaturation in the presence of Hsp90β. The 6P protein complex is composed of Hsp90, Hsp70, Hop, BAG1, Aha1 & Hsp40. JG98 (15 μM) is used as an inhibitor of Hsp70 and SEW84 (15 μM) and GA (15 μM) are used as inhibitors of Hsp90. The data is shown as percent (%) FLuc activity relative to the activity of FLuc prior to thermal denaturation. **B.** Bar graph depicting the normalized FLuc luminescence of transiently transfected HeLa cells

with FLuc variants (WT, L5 (R188Q) and L33 (R188Q; R261Q)) in the presence of the indicated concentration of SEW84. **C.** Cellular toxicity assay depicting the impact of the indicated concentration of SEW84 on the cellular ATP levels of HeLa cells transfected with the indicated FLuc. The data is normalized to the luminescent signal obtained in WT-transfected HeLa cells treated with DMSO. In all panels the error bars represent standard deviations ($n \geq 3$) and asterisks indicates $p < 0.05$ using a two-tailed t-test with the vehicle control used as a reference.

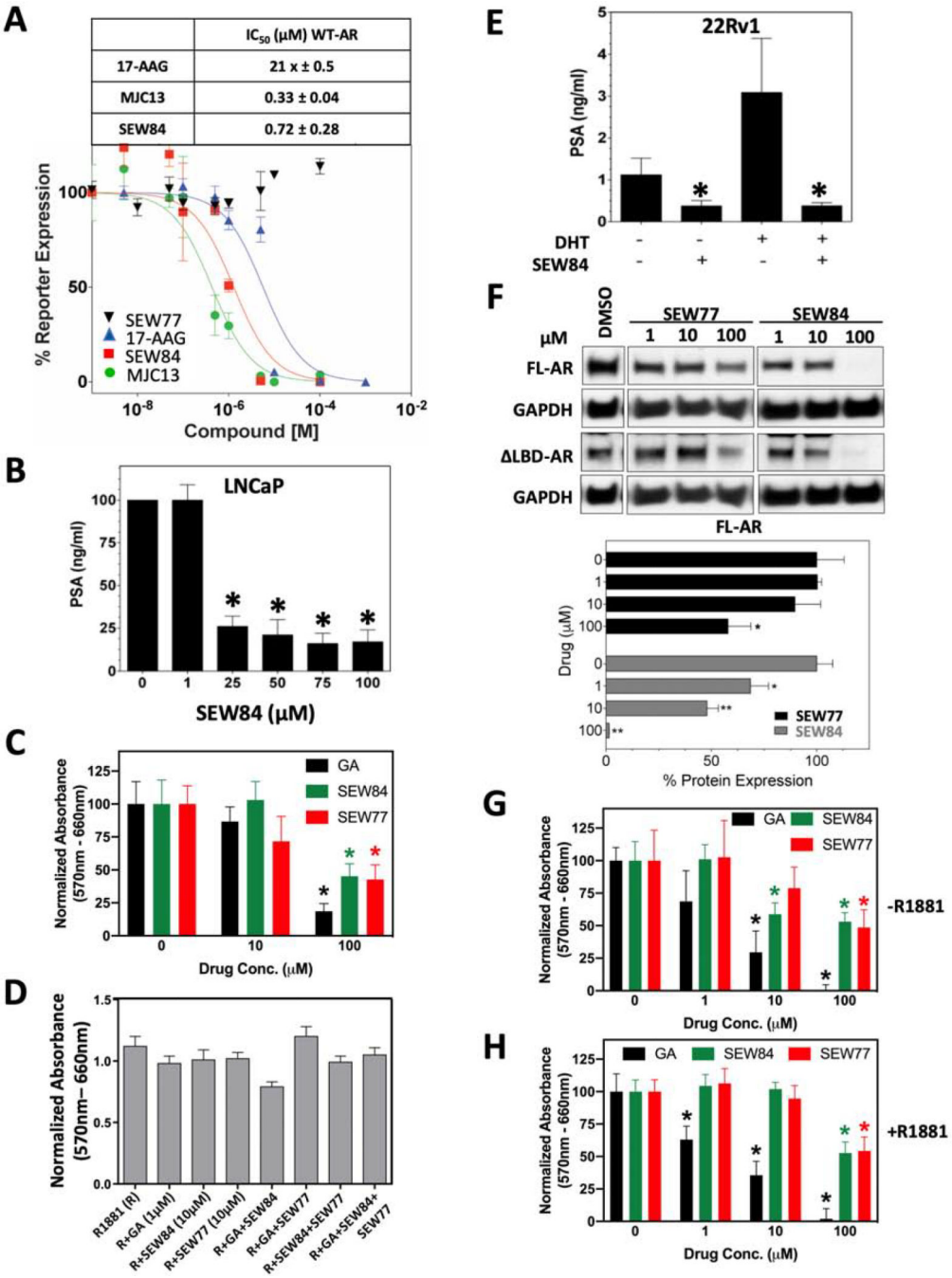

Figure 5. SEW84 inhibits the transcriptional activity of steroid hormone receptors.

A. Scatter plot showing the impact of SEW84 (red squares), 17-AAG (blue triangles), MJC13 (green circles) and SEW77 (black triangles) on the DHT-stimulated WT-AR-mediated transcriptional activity from the ARE-FLuc reporter in MDA-kb2 cells. Inset table depicts the IC50 values. **B.** Bar graph showing the impact of the indicated concentrations of SEW84 on the DHT-mediated expression of prostate specific antigen (PSA) in LNCaP cells. **C.** Bar graph depicting the normalized proliferation of LNCaP cells treated with the indicated compound. The data is shown as the mean ± SD (n = 3) normalized to the

absorption (570nm – 660nm) seen in the DMSO condition. **D.** Bar graph depicting the proliferation of LNCaP cells treated with the indicated compound(s). The data is shown as the mean absorption (570nm – 660nm) ± SD (n = 3). **E.** Bar graph showing the impact of SEW84 on the DHT-mediate expression of PSA by WT- or ΔLBD AR variants. **F.** Western blot of the full length (FL) AR and ΔLBD-AR from 22Rv1 cells treated with the indicated concentration of SEW77 or SEW84 in the presence of the synthetic DHT analog, R1881. A quantitation of the expression level of FL-AR in response to the indicated concentration of SEW77 or SEW84 is shown. The data are shown as mean ± SD normalized to the expression level seen in the DMSO treated control. **G.** Bar graph depicting the normalized proliferation of 22Rv1 cells treated with the indicated compound in the absence of R1881. The data is shown as the mean ± SD ($n \geq 3$) normalized to the absorption (570nm – 660nm) seen in the DMSO condition. **H.** Bar graph depicting the normalized proliferation of 22Rv1 cells treated with the indicated compound in the presence of R1881. The data is shown as the mean ± SD ($n \geq 3$) normalized to the absorption (570nm – 660nm) seen in the DMSO condition. In all panels the asterisks indicates $p < 0.05$ using a two-tailed t-test with the vehicle used as a reference.

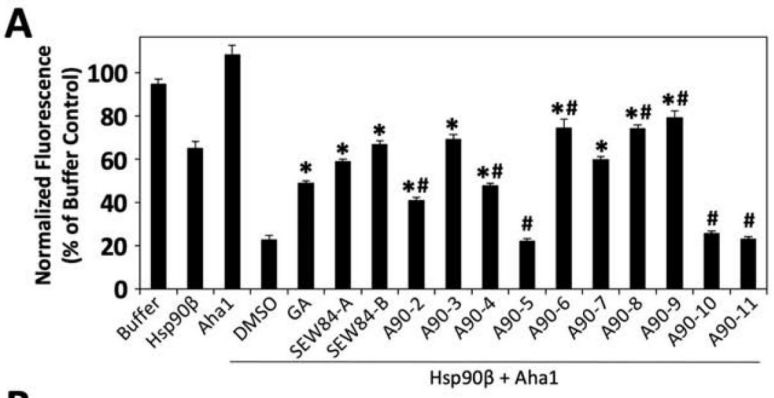

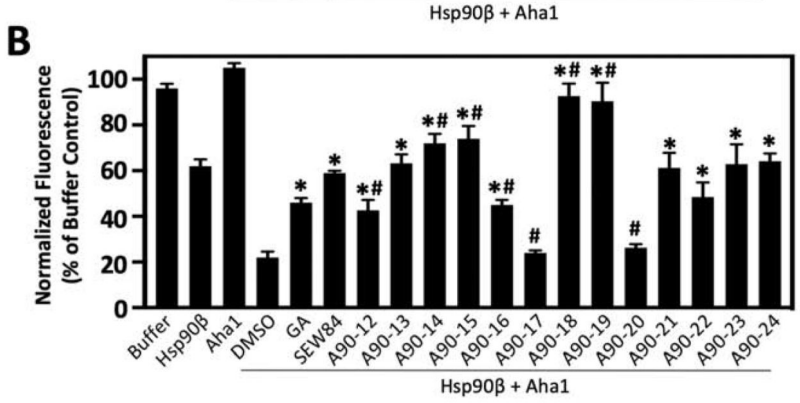

C

Compound	IC_{50} (μM)	Compound	IC_{50} (μM)
Hsp90		A90-12	13.2
Hsp90/Aha1		A90-13	5.2
SEW84	2.3	A90-14	5.9
A90-2	12.7	A90-15	4.9
A90-3	1.0	A90-16	4.5
A90-4	15.4	A90-17	18000
A90-5	N/A	A90-18	3.5
A90-6	0.5	A90-19	3.8
A90-7	7.0	A90-20	147
A90-8	3.8	A90-21	6.4
A90-T9	1.7	A90-22	31.1
A90-10	N/A	A90-23	8.9
A90-11	N/A	A90-24	3.6

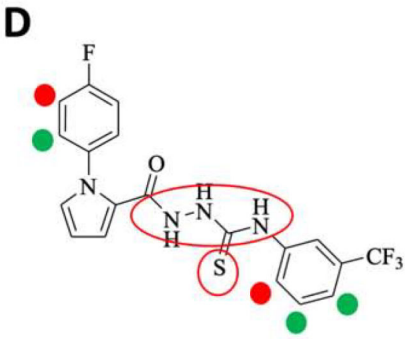

Figure 6. SAR analyses identifies key structural elements in SEW84.

A-B. Bar graph depicting the normalized fluorescence of the ASH activity assay in the presence of DMSO, 50 μM GA or 20 μM of the indicated SEW84 analog (A90). **C.** Table depicting the IC_{50} values of the indicated compound. **D.** Chemical structure of SEW84 depicting the permissive (green) and inhibitory (red) changes allotted. In all panels the error bars represent standard deviations ($n \geq 3$). The asterisk indicates $p < 0.05$ using a two-tailed t-test with the vehicle control used as a reference and the hashtag represents $p < 0.05$ using a two-tailed t-test with the SEW84 used as a reference.

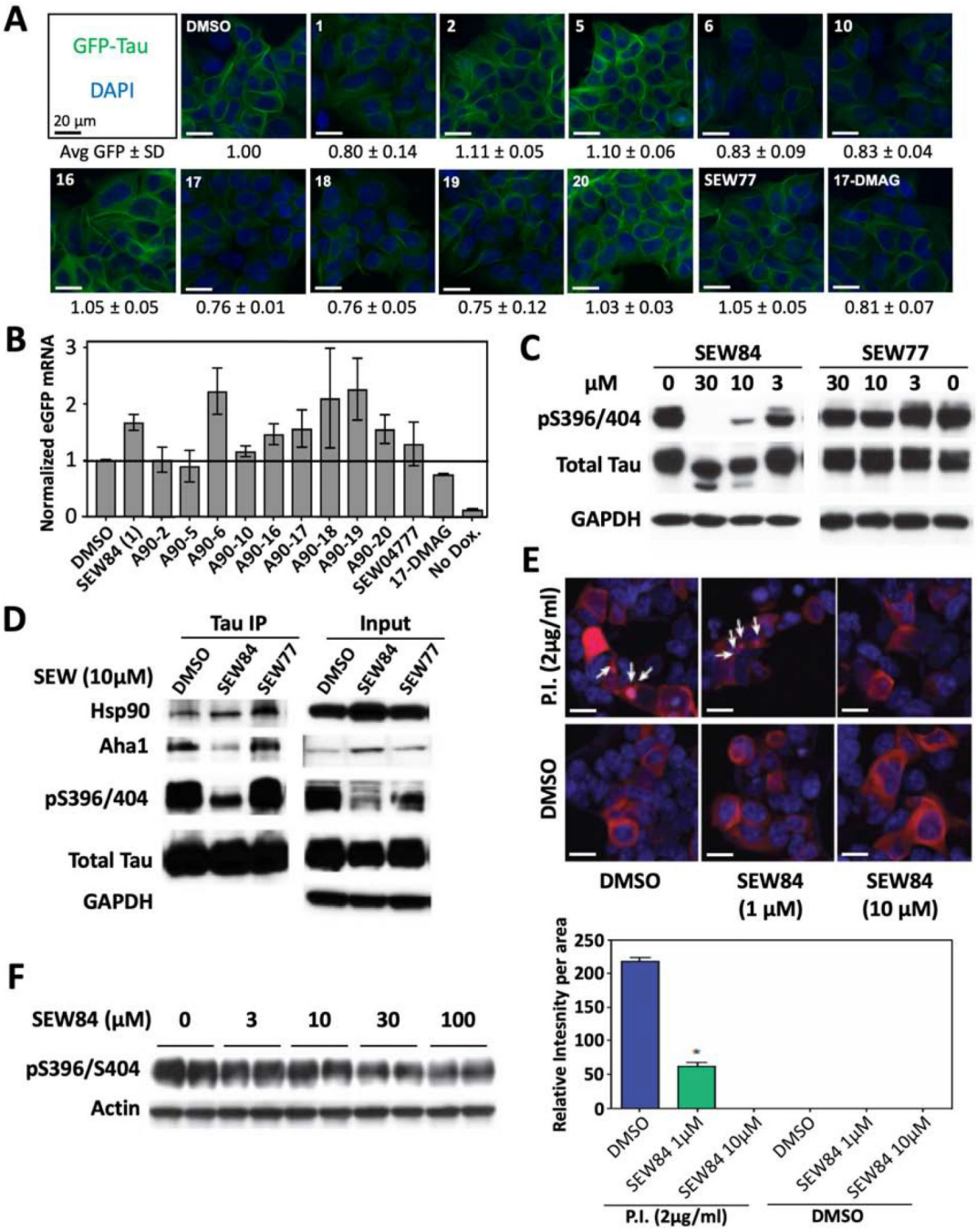

Figure 7. SEW84 clears toxic tau species *in vivo*.

A. Representative Immunofluorescence images of GFP-tau-0N4R HEK cells treated with 20 µM of the indicated A90 analog for 24h. The value shown represent the normalized mean intensity of GFP-Tau, which was normalized to that seen in the DMSO condition. The error values represent standard deviations (n ≥ 3). The scale bar is equal to 20 micrometers (µm) **B.** Bar graph depicting the mRNA level of eGFP in response to the treatment as in **A**. **C.** Representative Western blot analysis (n = 3) of tau-0N4R-HeLa cells treated with the indicated concentration of SEW84 or SEW77. **D.** Immunoblot analysis of tau

immunoprecipitates (left) from tau-0N4R-HeLa cells treated with 20 μM SEW84, 20 μM SEW77 or DMSO. **E.** Immunofluorescence (**upper panel**) of RFP-tau-0N4R HEK cells treated with protease inhibitor or DMSO in the presence or absence of the indicated concentration of SEW84. The white arrowheads indicate the location of RFP positive tau aggregates. The scale bar is equal to 20 micrometers (μm). The quantitative analysis (**lower panel**) provides the relative intensity per area for aggregated RFP-tau. The error bars represent standard deviations ($n \geq 3$). The asterisk indicates $p < 0.05$ using a two-tailed t-test with the vehicle control used as a reference. **F.** Western blot analysis of cultured brain slices prepared from transgenic mice expressing the P301L-tau variant and treated with the indicated concentration of SEW84.